Edinburgh Research Explorer

Choosing Stiffness and Damping for Optimal Impedance Planning

Choosing Stiffness and Damping for Optimal Impedance Planning

Mathew Jose Pollayil, Franco Angelini, Guiyang Xin, Michael Mistry, Sethu Vijayakumar,
Antonio Bicchi, *Fellow, IEEE,* and Manolo Garabini

Abstract—The attention given to impedance control in recent years does not match a similar focus on the choice of impedance values that the controller should execute. Current methods are hardly general and often compute fixed controller gains relying on the use of expensive sensors.

This paper addresses the problem of online impedance planning for Cartesian impedance controllers that do not assign the closed-loop inertia. We propose an optimization-based algorithm that, given the Cartesian inertia, computes the stiffness and damping gains without relying on force/torque measurements and so that the effects of perturbations are less than a maximum acceptable value. By doing so, we increase robot resilience to unexpected external disturbances while guaranteeing performance and robustness. The algorithm provides an analytical solution in the case of impedance-controlled robots with diagonally dominant inertia matrix. Instead, established numerical methods are employed to deal with the more common case of non-diagonally dominant inertia.

Our work attempts to create a general impedance planning framework, which needs no additional hardware and is easily applicable to any robotic system. Through experiments on real robots, including a quadruped and a robotic arm, our method is shown to be employable in real-time and to lead to satisfactory behaviors.

Index Terms—Impedance, Planning, Control.

(Corresponding Author: M. J. Pollayil)

M. J. Pollayil and A. Bicchi are with the Centro di Ricerca "Enrico Piaggio", Università di Pisa, Pisa 56126, Italy, with the Soft Robotics for Human Cooperation and Rehabilitation, Fondazione Istituto Italiano di Tecnologia, Genova 16163, Italy, and also with the Dipartimento di Ingegneria dell'Informazione, Università di Pisa, Pisa 56126, Italy (e-mail: mathewjose.pollayil@phd.unipi.it; antonio.bicchi@unipi.it).

F. Angelini and M. Garabini are with the Centro di Ricerca "Enrico Piaggio", Università di Pisa, Pisa 56126, Italy, and also with the Dipartimento di Ingegneria dell'Informazione, Università di Pisa, Pisa 56126, Italy (e-mail: frncangelini@gmail.com; manolo.garabini@unipi.it).

G. Xin is with the School of Optoelectronic Engineering and Instrumentation Science, Dalian University of Technology, Dalian, China. (e-mail:guiyang.xin@dlut.edu.cn).

M. Mistry and S. Vijayakumar are with the IPAB, School of Informatics, The University of Edinburgh, 10 Crichton Street, Edinburgh, EH8 9AB, United Kingdom (e-mail: guiyang.xin@ed.ac.uk; mmistry@ed.ac.uk; sethu.vijayakumar@ed.ac.uk).

This paper has supplementary downloadable material available at http://ieeexplore.ieee.org, provided by the authors.
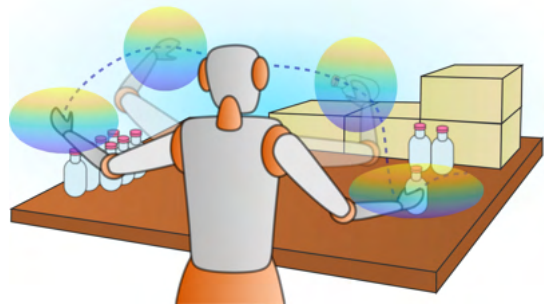
Figure 1. Planning a variable impedance, based on requirements on tracking and robustness, shapes the impedance ellipsoid and ensures better performance.

I. INTRODUCTION

In recent years, robots have been required to operate in environments where safety and performance are both tight requisites. In this regard, collaborative robots (*cobots*) are being adopted into several branches of the industry [1] to perform tasks such as shared manipulation [2] or on-site inspection [3]. Such robots are often built using compliant elements, such as soft coverings or springs, which enable safer operation modes that make it easier for humans and machines to coexist in working environments.

In addition to the robots with built-in compliance, i.e., soft robots [4], such as the ones with flexible joints/links [5], [6] or employing variable stiffness/impedance actuators [7], [8], also traditional "rigid" robots can be made compliant by enforcing a desired impedance behavior by means of control. Such a possibility is provided by the impedance control technique, initially proposed by Hogan [9] and later expanded by several authors, e.g., see [10], [11]. This control method offers the advantage of being able to modulate the impedance of the robot, which, together with proper tuning, can lead to improved efficiency and robustness. Therefore, employing impedance control on robots has become common.

This notwithstanding, very few authors have explicitly addressed the problem of choosing the desired impedance parameters: Section II highlights the context we refer to and presents a review of the relevant literature on the topic. One of the major challenges in computing the impedance gains lies in their tight dependency on the requirements of the specific tasks to be performed. As a result, using fixed offline-computed gains is rarely a good choice and, thus, the possibility of varying the impedance becomes interesting [12].

Nevertheless, current variable impedance planning techniques are very much application-oriented and rely on the use of expensive devices, such as force/torque sensors (cf. Section II-B). Additionally, these techniques often assume that the impedance controller performs inertia shaping, i.e., the controller assigns an arbitrary close-loop inertia. However, inertia shaping is not easily realizable in practice whenever expensive and very precise force/torque sensors are not available or if forces cannot be effectively measured [10]. For these reasons, current impedance planning methods are hardly useable out of their contexts.

In this paper, by substantially extending our previous work [13], we present a general algorithm that provides a framework to autonomously manage the planning of the impedance gains, stiffness and damping, of a Cartesian impedance controller. It attempts to minimize the effects of impacts/perturbations while ensuring tracking performance. The algorithm resorts to two methods, which are in turn based on solving constrained optimization problems. We minimize an objective function, which depends on the impedance, subject to some constraints derived from performance requirements. Without relying on external force/torque measurements to react at impact time, our approach performs a conservative design of the controller gains to always assign the minimum closed-loop inertia.

The proposed algorithm can handle both the cases of diagonally dominant and non-diagonally dominant Cartesian inertia matrices. Both can occur whenever inertia shaping cannot be performed. Hence, our approach aids in designing the impedance for a relevant class of impedance-controlled robotic systems, such as humanoids or quadrupeds, in which accurate measurements of external forces are often not available, and also for robotic manipulators that do not have precise built-in force/torque sensors.

The primary contribution of the present paper with respect to [13] is the overcoming of its main limitation: therein, planning was restricted to the case of diagonal inertia matrix. The possibility of using the same algorithm in the case of inertia matrices with negligible off-diagonal elements was discussed in [13]. Instead, the algorithm presented herein is general and can also deal with the non diagonal case, while including also the method presented in [13].

As a matter of fact, contrarily to [13], the planning framework that we propose in the present paper is not limited to specific systems, but addresses every robotic system in which impedance control is used. The results of experiments on a quadruped, which have been presented in [13], and on a robotic arm support the general nature of our effort. For this reason, this work can be considered as a general framework for impedance planning.

The paper is organized as follows: Section II-A provides the context for our work with a quick overview of impedance control. In Section II-B, a review of the literature on impedance design for robots is conducted. Section III states the problem we wish to tackle, for which a general optimization-based procedure and two approaches for its solution are presented in Sections IV, V, and VI, respectively. These lead to our impedance planning algorithm explained in Section VII. Then, in Section VIII, the proposed method is validated through

experiments on real robots and comparisons with a standard method. Finally, conclusions are drawn in Section IX.

II. STATE OF THE ART

A. Background

Let the dynamic model of a rigid-joint robotic system be

$$B(q)\ddot{q} + C(q,\dot{q})\dot{q} + G(q) = \tau + J^{\mathsf{T}}(q)F_{\text{ext}}, \qquad (1)$$

where $q \in \mathbb{R}^{n_j}$ is the vector of joint positions, $\tau \in \mathbb{R}^{n_j}$ is the vector of joint torques, $B \in \mathbb{R}^{n_j \times n_j}$ is the mass matrix, $C \in \mathbb{R}^{n_j \times n_j}$ is the Coriolis and centrifugal matrix, $G \in \mathbb{R}^{n_j}$ is the vector of gravity torques, $J \in \mathbb{R}^{6 \times n_j}$ is the analytic Jacobian of the end-effector, and $F_{\text{ext}} \in \mathbb{R}^6$ is the external force/torque acting on the end-effector. We wish to impose a closed-loop impedance model of the form

$$\Lambda_{\text{d}}\ddot{\tilde{x}} + D_{\text{d}}\dot{\tilde{x}} + K_{\text{d}}\tilde{x} = F_{\text{ext}}, \qquad (2)$$

where $\tilde{x} = x - x_{\text{d}}$ is the deviation of the end-effector pose $x \in \mathbb{R}^6$ from the desired equilibrium pose $x_{\text{d}} \in \mathbb{R}^6$. The matrices $\Lambda_{\text{d}} \in \mathbb{R}^{6 \times 6}$, $D_{\text{d}} \in \mathbb{R}^{6 \times 6}$ and $K_{\text{d}} \in \mathbb{R}^{6 \times 6}$ are respectively the desired positive-definite Cartesian inertia, damping, and stiffness. Notice that, using the geometric Jacobian would reduce the issue of singularity prone representations of orientation. However, this might require appropriately redefining $\tilde{x}$ [14].

For instance, the behavior in (2) can be achieved using the following control law [10]:

$$\tau = J^{\mathsf{T}}(q)F_\tau + C(q,\dot{q})\dot{q} + G(q), \qquad (3)$$

with the control input $F_\tau \in \mathbb{R}^6$ being

$$\begin{aligned} F_\tau &= \Lambda(q)\ddot{x}_{\text{d}} - \Lambda(q)\Lambda_{\text{d}}^{-1}(D_{\text{d}}\dot{\tilde{x}} + K_{\text{d}}\tilde{x}) \\ &\quad + (\Lambda(q)\Lambda_{\text{d}}^{-1} - I)F_{\text{ext}} - \Lambda(q)\dot{J}(q)\dot{q}, \end{aligned} \qquad (4)$$

where $\Lambda(q) = \left(J(q)B^{-1}(q)J^{\mathsf{T}}(q)\right)^{-1}$ is the robot equivalent Cartesian inertia matrix. Please note that (3)-(4) is merely one of the many possible impedance controllers. Depending on the system under analysis, different implementations (e.g., [15], [16], [17], [18], [19]) can be employed, leading to closed loop dynamics analogous to (2). It is worth mentioning that, according to the choice of the Jacobian, the impedance of not only the end-effector but multiple points of the robot can be regulated. However, this might be feasible only to the extent allowed by the degrees of freedom of the system.

Additionally, notice how the model-based control law (3)-(4) neglects delays and static nonlinearities that permeate the real hardware. These are often assumed to be negligible or the controller fast enough to compensate for them. However, under such assumptions control law (3)-(4) guarantees to assign the closed-loop behavior (2). The actual behavior of the controlled system will depend on whether its real dynamics is faster than the one that excites it, i.e. F_{ext}.

If we wish to find Λ_{d}, D_{d}, and K_{d} so that the impedance is minimized and the tracking performance is guaranteed, this can be done without big effort since inertia shaping is performed: in (2) all matrices are arbitrarily assigned and, hence, can be chosen to be diagonal for enforcing an exact

decoupled behavior. As a matter of fact, most of the traditional stiffness and damping design methods for single degree of freedom second order systems can be applied.

However, in practice, assigning an arbitrary Λ_{d} is not always trivial. Whenever it is not possible to employ sensors that provide precise and direct feedback of the external forces or Cartesian acceleration, the closed-loop inertia cannot be shaped. Force/torque sensors are not only expensive but usually have limited measurement areas, out of which forces are not sensed effectively. Moreover, acquiring accurate measurements of the robot acceleration is also hard.

Without such feedback, the Cartesian inertia needs to be set identical to the robot Cartesian inertia $\Lambda(q)$ [10], [16]. Moreover, since the inertia is not constant anymore, if the impedance model is meant to represent a real mechanical system, a non-constant term $\bar{C}(q, \dot{q})$ should also be introduced[1].

The control input (4) can be changed as

$$F_\tau = \Lambda(q)\ddot{x}_{\mathrm{d}} - D_{\mathrm{d}}\dot{\tilde{x}} - K_{\mathrm{d}}\tilde{x} - \bar{C}(q,\dot{q})\dot{\tilde{x}} - \Lambda(q)\dot{J}(q)\dot{q}. \quad (5)$$

Here, $\bar{C}(q, \dot{q})$ can be any matrix such that $\dot{\Lambda}(q) - 2\bar{C}(q, \dot{q})$ is skew symmetric (e.g., $\bar{C} = \frac{1}{2}\dot{\Lambda}$) [10].

Using (3) together with (5), the following closed-loop nonlinear impedance behavior is achieved:

$$\Lambda(q)\ddot{\tilde{x}} + (D_{\mathrm{d}} + \bar{C}(q,\dot{q}))\dot{\tilde{x}} + K_{\mathrm{d}}\tilde{x} = F_{\mathrm{ext}}. \quad (6)$$

The presence of the term $\bar{C}(q, \dot{q})$ is usually a hindrance for the design of the controller gains D_{d} and K_{d}. This is usually solved by assuming slowly varying inertia ($\dot{\Lambda}(q) \approx 0$) [10] whenever the velocity of the robot is not high, or if the controller itself (or a lower level controller) compensates $\bar{C}(q, \dot{q})$. With this assumption, several approaches have been proposed in the literature to design the impedance parameters.

B. Literature Review

Traditionally, the choice of the gains for impedance control is based on the common rationale of considering a trade-off between permissible interaction forces and allowable set-point errors. Initially, such an analysis, led to the outlining of fundamental impedance planning strategies, such as the ones presented in [20]. Therein, the authors carried out some basic discussions about choosing optimal values of impedance, based on well-known results in linear optimal control theory.

Soon enough, the option of varying the target impedance for ensuring stability of interaction emerged. For instance, [21] examined the importance of the target damping ratio, which was found to be a critical factor for contact stability with stiff environments. This study also brought about the idea of a fuzzy adaptation of the impedance based on deviations of the measured force from the desired ones in order to limit peaks in contact forces [22].

Adaptive and iterative learning controls allow tackling the problem of planning impedance. For example, [23] proposed an adaptive progressive learning method based on measurements of error and reaction forces for real-time tuning of stiffness and damping. More recently, iterative learning control

---

[1]This aids in proving the asymptotic convergence of the error $\tilde{x}(t)$.

has been consistently used to shape impedance. Examples are [24] and [25]. The former dealt with combining iterative learning control with an adaption of the stiffness for enabling its convergence to an optimal value. Instead, the latter proposed an iterative algorithm to smooth the damping for minimizing the external force exerted by a human. Another relevant work is [26], which presented a novel controller that deals with periodic tasks by estimating interaction forces, and by adapting feed-forward force and impedance, but also by modifying the reference trajectory to deal with rigid environments. Two very recent works are also noteworthy: [27] approaches optimal control through model predictive impedance control and [28] derives passivity conditions that provide bounds on the desired impedance gains.

Control algorithms can also be combined with other techniques, such as programming by demonstration, to learn impedance parameters while coping with unmodelled uncertainties. For instance, [29] used haptic and proprioceptive feedback to tune the impedance for accurate reproduction of learned tasks. Another example of impedance learning method based on human demonstrations is [30], in which tactile sensors were used to modulate the gains of object-level impedance control to accomplish robust and dexterous manipulation. A human-like adaptive learning tool, which does not require interaction force sensing and that is able to deal with periodic tasks also in presence of unstable interactions, was proposed in [31]. In [32], a combination of Gaussian Mixture Model and LQR control was used to reproduce stiffness geometry obtained from human demonstrations.

Besides adaptive and iterative learning, also machine learning algorithms can deal with impedance planning. A very early example of application of neural networks to the regulate end-effector impedance for minimizing position/force control error can be seen in [33]. In [34], the authors presented an application of reinforcement learning PI^2 algorithm to find the impedance necessary to accomplish a given task. Despite their efficacy, the price to pay is that learning techniques require huge datasets and a large number of trials for properly learning optimal models [35].

Optimization-based techniques have also been proposed. In [36], particle swarm optimization was used to tune offline the impedance controller. We proposed robust optimization-based design of system compliance and impedance, respectively, in [37] and [13]. We also presented optimal control-based formulations to algorithmically optimize the spatio-temporal modulation of impedance in [38], [39] and applied it for mapping human impedance strategies to heterogeneous robot actuators [40] and realising explosive movement tasks [41]. Another example of particle swarm optimization is [42]. Therein, the target impedance of an exoskeleton was optimized for assistance and rehabilitation in accordance with the knowledge of an estimate of human impedance.

Approaches specifically targeted at human-robot interaction are also topics of research interest. Most of these are based on measurements of the forces applied by the human. For instance, [43] and [44] changed the impedance based on a passivity index and an estimation of the human stiffness, respectively. A different approach was presented in [45]:

(a) Constant force disturbance with low impedance.

(b) Environment interaction with low impedance.

(c) Constant force disturbance with high impedance.

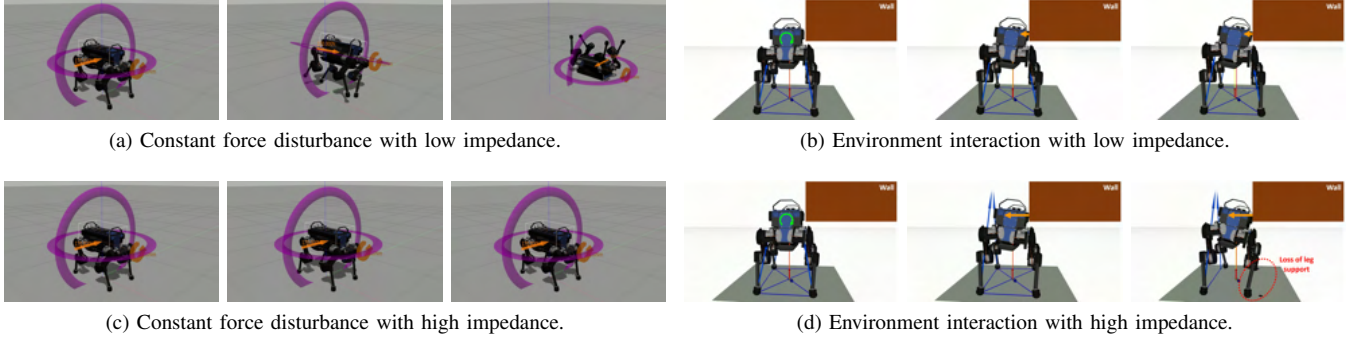(d) Environment interaction with high impedance.

Figure 2. High impedance vs low impedance on the robot ANYmal with a Cartesian impedance controller regulating its torso. With low impedance, when subject to an external force disturbance, the robot cannot track correctly the reference position and falls. However, more robustness to unforeseen contacts is displayed. High impedance, instead, ensures tracking by rejecting force disturbances, but environment interaction destabilizes the robot, which loses support on two legs (dashed red circle).
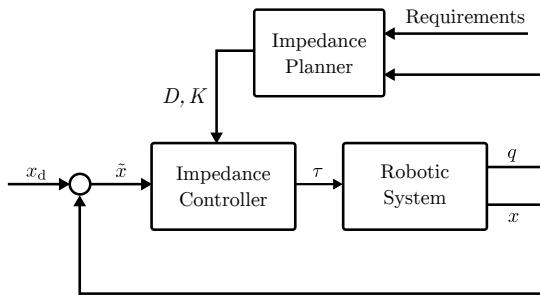

Figure 3. The proposed algorithm acts by modifying the gains K and D of the impedance controller based on the current state q of the robot and on some performance requirements (explained later on).

therein, an experimental study on human-robot comanipulation was carried out and the end-effector dynamics is controlled to a mass-damper behavior. The damping matrix is changed as a function of the end-effector velocity in order to improve accuracy and execution time of the collaborative task.

Some other works are also worth citing. In [46], [47] and [48], the authors used the concept of Lyapunov stability margins to regulate the impedance for improved balancing and walking in humanoids. Finally, [49] and [50] employed force measurements and visual data to auto-tune the impedance.

The approach proposed in the present paper is novel with respect to the majority of the state of the art in the following: 1) it does not require the use of any force/torque sensors; 2) it builds on top of established results in control theory and optimization and is not related to any specific robotic system or controller; 3) it provides robustness by performing a worst-case design of the controller gains. These points are confirmed through experimental validation and comparisons with a standard method for impedance planning with inertia shaping (see Section VIII).

III. PROBLEM DESCRIPTION

As mentioned in Section II-A, with the assumption of slowly varying inertia, the closed-loop impedance without inertia shaping (6) becomes

$$\Lambda(q)\ddot{\tilde{x}} + D\dot{\tilde{x}} + K\tilde{x} = F_{\text{ext}}. \tag{7}$$

Here, and also in the remaining of the paper, for the sake of compactness, we remove the subscript d to both K and

D. Notice that the only difference with (2) is that Λ is configuration dependent and usually not diagonal, and non modifiable. Recall that, since $\Lambda(q)$ is time-varying, constant positive-definite controller gains might not suffice for the convergence of (7).

We wish to address the following problem. Let some bounds be provided on the matrices K and D; these can be related to the limits on the actuation and on the degree of uncertainty in the dynamic model (see also Appendix C). Provided also some limits on the initial states $\tilde{x}_0$ and $\dot{\tilde{x}}_0$, and on the external forces F_{ext}, find an algorithm that autonomously chooses the values of K and D such that the evolution of the tracking error $\tilde{x}$ remains bounded in between some required values. Moreover, we demand that the impedance assigned by the controller should be the lowest possible that fulfills the stated requirements. This is because we wish to be robust to unexpected contacts with external factors, such as the environment.

This problem clearly requires a solution that is a trade-off between high and low impedance. A low closed-loop impedance improves robustness to undesired and unexpected disturbances; a high impedance increases tracking performance (see Figure 2 for an example) [14]. Since, we require both robustness and good tracking, the solution to our problem should be somewhere in between high and low gains.

Finding such a solution would be fairly easy if inertia shaping were performed since decoupled shaping of each subsystem could be conducted. Instead, in our case, traditional methods fail in providing a general solution to the stated stiffness and damping planning problem because of the couplings in the system, caused by non-diagonal inertia, and also since we assume not to use any force/torque sensor (see the literature review in Section II-B). Notice that tuning the large number of parameters of K and D by trial and error while complying with constraints on positive definiteness of the matrices, on the boundedness of tracking error, and on minimizing the impedance is practically never viable.

It is also worth discussing that minimizing the impedance is one possible way to achieve the aforementioned desired behavior. Some other viable solutions include regulating the inner control loops of the robot to quickly react to impacts or

adding kinetic energy constraints directly into the controller formulation. Also mechanically modifying the robot to include soft paddings on the covers can help. However, these solutions do not fit into the scope of this paper, which extends our previous work [13] within the context of impedance control.

IV. PROPOSED SOLUTION

The basic idea behind our approach to the problem is to provide the controller - which realizes (7) - with the minimum necessary impedance gains, K and D, for achieving the required performance in presence of bounded external disturbances. This is the aim of our impedance planner, which will act on the whole architecture as shown in Figure 3.

We set up an optimization problem aimed at computing at each planning iteration the minimum impedance in accordance with the current state of the robot and with some provided performance and robustness bounds.

$$\begin{aligned}
\underset{D,K}{\arg\min} \quad & h(D,K) \\
\text{s.t.} \quad & l_{d_{i,j}} \leq d_{i,j} \leq u_{d_{i,j}} \\
& l_{k_{i,j}} \leq k_{i,j} \leq u_{k_{i,j}} \\
\text{s.t.} \quad & \max_{\tilde{x}_0, \dot{\tilde{x}}_0, F_{\text{ext}}} |\tilde{x}_i(t)| \leq b_i \quad \forall t \in [0, +\infty) \\
& l_{\tilde{x}_{0_i}} \leq \tilde{x}_{0_i} \leq u_{\tilde{x}_{0_i}} \\
& l_{\dot{\tilde{x}}_{0_i}} \leq \dot{\tilde{x}}_{0_i} \leq u_{\dot{\tilde{x}}_{0_i}} \\
\text{s.t.} \quad & l_{F_{\text{ext}_i}} \leq F_{\text{ext}_i} \leq u_{F_{\text{ext}_i}} \\
& \Lambda(q)\ddot{\tilde{x}} + D\dot{\tilde{x}} + K\tilde{x} = F_{\text{ext}}.
\end{aligned} \quad (8)$$

The solution to (8) finds the D and K, which minimize h, and ensure that the error $\tilde{x}$ remains bounded throughout time, by keeping the peaks of each $\tilde{x}_i(t)$ below the bounds b_i, provided that the external force F_{ext} and the initial conditions $\tilde{x}_0$ and $\dot{\tilde{x}}_0$ are bounded. This constraint on the peak of the error will be denoted also as *performance requirement* in the rest of the paper. The elements of the damping and stiffness matrices are $d_{i,j}$ and $k_{i,j}$, respectively. The bilateral bounds on the variables $d_{i,j}$, $k_{i,j}$, $\tilde{x}_0$, $\dot{\tilde{x}}_0$, and F_{ext} are written using the operators $l_{(\cdot)}$ and $u_{(\cdot)}$, which respectively denote lower and upper bounds.

Notice that (8) is a minimization problem with a maximization constraint, which needs to be solved $\forall t \in [0, +\infty)$ and $\forall i, j \in \{1, \ldots, 6\}$ (this detail is omitted also in the rest of the paper for the sake of compactness of equations). It is noteworthy that the maximization constraint in (8) is a function of unknown but bounded parameters, namely the initial conditions and external forces, which are uncertain. Problems such as (8) are commonly referred to as robust optimizations [51].

In this work, we choose to keep always at a minimum required value the impedance regulated by the controller. Hence, in (8), the cost function $h(D,K)$ is targeted at minimizing the impedance of (7) to increase resilience to external uncertainties while fulfilling the *performance requirement* through the maximization constraint. The impedance matrix of (7) is given by $Z(j\omega) = -\omega^2\Lambda + j\omega D + K$, where $\omega = 2\pi f$ and f is the frequency of the external force. For instance, we can choose

$$h_Z(D,K) = \|Z(j\omega)\|_F^2. \quad (9)$$

Here, the operator $\|\cdot\|_F$ stands for the Frobenius norm of a matrix. However, since we have no control both over the angular frequency ω and on the inertia Λ, to minimize (9), a best effort approach would be attempting to minimize

$$h(D,K) = \|\kappa D + K\|_F^2, \quad (10)$$

where κ is a constant coefficient for normalizing the different units in the cost.

To solve optimization (8), with the cost being (10), we make the following assumptions:

Assumption 1. $\Lambda(q)$ *is almost a constant* Λ *between two planning instances. Hence, we assume quasi-static conditions between two consecutive impedance updates.*

Assumption 2. *The external disturbances acting on the robotic system occur in brief instants of time. Thus, we approximate* F_{ext} *to be impulsive:* $F_{\text{ext},i} = \bar{F}\,\delta_{\text{d}}(t)$.

The first assumption is reasonable if the robot velocity is not high and if the gain update rate of the planner is relatively high. These are highly specific to the robot and can be estimated numerically if a symbolic expression of $\Lambda(q)$ is available. However, this tedious procedure can often be replaced by trial and error. The second assumption requires external forces to act only for short amounts of time, like in the case of impacts. However, these should not be ideal impulses with dynamics much faster than the control rate, which might prevent the desired impedance behavior to be assigned by the controller. We also disregard the case of very prolonged interactions.

Remark 1. *Suppose a constant force acting on the robot end-effector is due to an external body attached to it. If the inertial properties of the body are known, the robot dynamic model can be modified so that the controller compensates for the load. The result would be a change of the inertia* $\Lambda(q)$.

In line with Remark 1, in many practical scenarios, e.g., a robot manipulator grasping an object, Assumption 2 is not restrictive and external impacts can be considered impulsive.

Remark 2. *The impulse response of a linear system is equivalent to the free response from suitable non-zero initial conditions with* $\tilde{x}_0 \neq 0$ *[52] (see Appendix A). Hence, by virtue of* Assumption 2 *we limit ourselves to optimize the free response of* (7).

Assumption 1 and Remark 2 lead us to modify (8) into

$$\begin{aligned}
\underset{D,K}{\arg\min} \quad & h(D,K) \\
\text{s.t.} \quad & l_{d_{i,j}} \leq d_{i,j} \leq u_{d_{i,j}} \\
& l_{k_{i,j}} \leq k_{i,j} \leq u_{k_{i,j}} \\
\text{s.t.} \quad & \max_{\tilde{x}_0, \dot{\tilde{x}}_0} |\tilde{x}_i(t)| \leq b_i \quad \forall t \in [0, +\infty) \\
& l_{\tilde{x}_{0_i}} \leq \tilde{x}_{0_i} \leq u_{\tilde{x}_{0_i}} \\
\text{s.t.} \quad & l_{\dot{\tilde{x}}_{0_i}} \leq \dot{\tilde{x}}_{0_i} \leq u_{\dot{\tilde{x}}_{0_i}} \\
& \Lambda\ddot{\tilde{x}} + D\dot{\tilde{x}} + K\tilde{x} = 0.
\end{aligned} \quad (11)$$

Here, we recompute the bounds on $\dot{\tilde{x}}_0$ also in accordance with the removed bounds on F_{ext_i} (see Appendix A).

Equation (7) is usually not decoupled in six single degree of freedom equations to be solved independently. To find

$\tilde{x}_i(t)$, it is required to compute first $\tilde{x}(t)$ and then choose $\tilde{x}_i(t) = e_i^\mathsf{T} \tilde{x}(t)$, where e_i is the i$^{\text{th}}$ vector of the canonical basis. Let $\xi = \begin{bmatrix} \tilde{x}^\mathsf{T} & \dot{\tilde{x}}^\mathsf{T} \end{bmatrix}^\mathsf{T}$ and $\nu = F_{\text{ext}}$. System (7) can be re-written as

$$\dot{\xi} = \underbrace{\left[\begin{array}{c|c} O & I \\ \hline -\Lambda^{-1}K & -\Lambda^{-1}D \end{array}\right]}_{A} \xi + \underbrace{\left[\begin{array}{c} O \\ \hline \Lambda^{-1} \end{array}\right]}_{B} \nu. \quad (12)$$

The analytical solution of the homogeneous part of (12), in the general case of time-varying matrix $A(t)$, is given by

$$\xi(t) = \phi(t, t_0)\xi_0. \quad (13)$$

Here, $\phi(t, \tau)$ is called state-transition matrix and can be found using various methods: for more details refer [53]. However, via Assumption 1, $A(t)$ can be assumed constant, and (13) becomes $\xi(t) = \mathrm{e}^{At}\xi_0$. The error $\tilde{x}(t) = \begin{bmatrix} I & O \end{bmatrix}\xi(t)$ and its i$^{\text{th}}$ component $\tilde{x}_i(t) = e_i^\mathsf{T}\begin{bmatrix} I & O \end{bmatrix}\xi(t)$.

In the light of the above considerations, (11) becomes

$$\begin{aligned} &\operatorname*{arg\,min}_{D,K} \quad h(D,K) \\ &\quad \text{s.t.} \quad \begin{array}{l} l_{d_{i,j}} \leq d_{i,j} \leq u_{d_{i,j}} \\ l_{k_{i,j}} \leq k_{i,j} \leq u_{k_{i,j}} \end{array} \\ &\quad \text{s.t.} \quad \max_{\tilde{x}_0, \dot{\tilde{x}}_0} |e_i^\mathsf{T}\begin{bmatrix} I & O \end{bmatrix}\mathrm{e}^{At}\begin{bmatrix} \tilde{x}_0^\mathsf{T} & \dot{\tilde{x}}_0^\mathsf{T} \end{bmatrix}^\mathsf{T}| \leq b_i \quad (14) \\ &\qquad\qquad\qquad t \geq 0 \\ &\quad \text{s.t.} \quad \begin{array}{l} l_{\tilde{x}_{0_i}} \leq \tilde{x}_{0_i} \leq u_{\tilde{x}_{0_i}} \\ l_{\dot{\tilde{x}}_{0_i}} \leq \dot{\tilde{x}}_{0_i} \leq u_{\dot{\tilde{x}}_{0_i}}. \end{array} \end{aligned}$$

As such, this optimization problem is robust and non-convex due to the uncertainties and the dependence on time in the maximization constraint. Hence, this approach is not easily viable. It is more practical to solve the maximization for making optimization (12) deterministic. A straightforward way is by enforcing a decoupled behavior.

Two cases can be identified. Let m_{ij} denote the entry in the i$^{\text{th}}$ row and j$^{\text{th}}$ column of Λ: we distinguish the following.

Case 1. *Diagonally Dominant Inertia:*

$$|m_{ii}| \geq \sum_{i \neq j} |m_{ij}| \quad \forall i, j.$$

Case 2. *Non-diagonally Dominant Inertia:*

$$\exists i \text{ such that } |m_{ii}| < \sum_{i \neq j} |m_{ij}| \quad \forall j.$$

In the following, the former case is tackled in Section V, while the latter is addressed in Section VI.

V. CASE 1: DIAGONALLY DOMINANT INERTIA

As discussed in [13], for some robots and control choices, the Cartesian inertia matrix Λ can be diagonally dominant. This is the case, for example, when the controller is set to modulate the impedance of the torso of a quadruped. The large inertia of the robot base would make the elements on the diagonal of Λ dominant w.r.t. the off-diagonal terms.

A. Decoupled Optimization

For diagonally dominant Λ, we replace it with its diagonal approximation. We choose D and K to be diagonal as well. This yields the decoupled approximation of (7)

$$m_i\ddot{\tilde{x}}_i + d_i\dot{\tilde{x}}_i + k_i\tilde{x}_i = F_{\text{ext},i}. \quad (15)$$

Here, $m_i = m_{ii}$, d_i and k_i are the i$^{\text{th}}$ diagonal elements, respectively, of the constant diagonally dominant Λ, of D and of K. The scalars $\tilde{x}_i$, $\dot{\tilde{x}}_i$ and $\ddot{\tilde{x}}_i$ are the i-th elements of $\tilde{x}$, $\dot{\tilde{x}}$ and $\ddot{\tilde{x}}$, respectively. $F_{\text{ext},i}$ is i$^{\text{th}}$ element of F_{ext}.

As a consequence, (11) becomes decoupled into six distinct optimizations if we choose the cost $h(D, K)$ to be independent for each subsystem. Hence, by choosing the cost for the i$^{\text{th}}$ subsystem as $h_i(d_i, k_i)$, optimization (11) turns out to be

$$\begin{aligned} &\operatorname*{arg\,min}_{d_i, k_i} \quad h_i(d_i, k_i) \\ &\quad \text{s.t.} \quad \begin{array}{l} l_{d_i} \leq d_i \leq u_{d_i} \\ l_{k_i} \leq k_i \leq u_{k_i} \end{array} \\ &\quad \text{s.t.} \quad \max_{\tilde{x}_{0_i}, \dot{\tilde{x}}_{0_i}} |\tilde{x}_i(t)| \leq b_i \qquad \forall t \in [0, +\infty) \quad (16) \\ &\quad \text{s.t.} \quad \begin{array}{l} l_{\tilde{x}_{0_i}} \leq \tilde{x}_{0_i} \leq u_{\tilde{x}_{0_i}} \\ l_{\dot{\tilde{x}}_{0_i}} \leq \dot{\tilde{x}}_{0_i} \leq u_{\dot{\tilde{x}}_{0_i}} \\ m_i\ddot{\tilde{x}}_i + d_i\dot{\tilde{x}}_i + k_i\tilde{x}_i = 0, \end{array} \end{aligned}$$

$\forall i \in \{1, \cdots, 6\}$, i.e., for each subsystem.

We enforce one of the three behaviors of second order linear systems: in particular, we choose the *critically-damped* condition,

$$k_i = \frac{d_i^2}{4m_i}, \quad (17)$$

which guarantees the fastest convergence of the error without oscillations. Here, since the stiffness becomes a function of the damping, the optimization is performed only over d_i. Thus, for instance, $h_i(d_i, k_i)$ can be chosen as a quadratic function of d_i. Moreover, by taking into account the analytical solution of (15) for impulsive external forces [52] (by virtue of Assumption 2 and Remark 2), and defining the worst case initial conditions

$$\begin{aligned} \tilde{x}_{0_i,\max} &\triangleq \max(|l_{\tilde{x}_{0_i}}|, u_{\tilde{x}_{0_i}}), \\ \dot{\tilde{x}}_{0_i,\max} &\triangleq \max(|l_{\dot{\tilde{x}}_{0_i}}|, u_{\dot{\tilde{x}}_{0_i}}), \end{aligned} \quad (18)$$

optimization (16) can be re-written as

$$\begin{aligned} &\operatorname*{arg\,min}_{d_i} \quad d_i^2 \\ &\quad \text{s.t.} \quad l_{d_i} \leq d_i \leq u_{d_i} \\ &\quad \text{s.t.} \quad \max_{\tilde{x}_{0_i}, \dot{\tilde{x}}_{0_i}, t} \left(\tilde{x}_0 + \left(\dot{\tilde{x}}_0 + \frac{\tilde{x}_0 d_i}{2m_i}\right)t\right)\mathrm{e}^{-\frac{d_i t}{2m_i}} \leq b_i \\ &\qquad\qquad 0 \leq \tilde{x}_{0_i} \leq \tilde{x}_{0_i,\max} \\ &\quad \text{s.t.} \quad 0 \leq \dot{\tilde{x}}_{0_i} \leq \dot{\tilde{x}}_{0_i,\max} \\ &\qquad\qquad t \geq 0. \end{aligned} \quad (19)$$

We transform the robust optimization problem into a deterministic one. To this end, we solve the maximization constraint, Using KKT conditions [54], and replace it in (19) with the following nonlinear inequality:

$$\frac{2m_i\dot{\tilde{x}}_{0_i,\max} + d_i\tilde{x}_{0_i,\max}}{d_i}\mathrm{e}^{\left(\frac{-2m_i\dot{\tilde{x}}_{0_i,\max}}{2m_i\dot{\tilde{x}}_{0_i,\max} + d_i\tilde{x}_{0_i,\max}}\right)} \leq b_i. \quad (20)$$

This can be further simplified by finding a conservative linear upper-bound, such as

$$\max_{\tilde{x}_{0_i}, \dot{\tilde{x}}_{0_i}, t} \tilde{x}_i(t) \leq \tilde{x}_{0_i,\max} + \frac{2\,m_i\,\dot{\tilde{x}}_{0_i,\max}}{\mathrm{e}\,d_i}. \tag{21}$$

This maximum represents the peak that the free response of (15) would reach from the worst-case initial conditions $(\tilde{x}_{0_i,\max}, \dot{\tilde{x}}_{0_i,\max})$. By using (21), optimization (19) turns into

$$\begin{aligned} \arg\min_{d_i} \quad & d_i^2 \\ \text{s.t.} \quad & l_{d_i} \leq d_i \leq u_{d_i} \\ \text{s.t.} \quad & d_i \geq \frac{2\,m_i\,\dot{\tilde{x}}_{0_i,\max}}{(b_i - \tilde{x}_{0_i,\max})\,e}, \end{aligned} \tag{22}$$

which has the following closed form solution [13]:

$$d_i = \min\left(\max\left(l_{d_i}, \frac{2\,m_i\,\dot{\tilde{x}}_{0_i,\max}}{(b_i - \tilde{x}_{0_i,\max})\,\mathrm{e}}\right), u_{d_i}\right). \tag{23}$$

For better explanations and lines of proof of the previous steps, please refer to [13].

Equation (23) together with (17) provides two direct formulae to compute the optimal damping and stiffness to achieve a critically damped behavior with minimum impedance and that complies with the *performance requirement*. However, since we considered only a single planning iteration so far, the stability of the closed loop system (15) with time varying gains remains to be studied.

B. Stability Analysis

Given the second order linear time-varying system

$$m_i(t)\ddot{\tilde{x}} + d_i(t)\dot{\tilde{x}} + k_i(t)\tilde{x} = 0, \tag{24}$$

the stability of its equilibrium in the origin for the critically-damped case (17) can be verified by the following:

Theorem 1. *The origin of* (24) *is uniformly asymptotically stabile in the critically-damped case if,* $\forall t \geq 0$, $d_i(t)/m_i(t)$ *is positive, bounded and differentiable, and*

$$\dot{d}_i(t) > -\frac{d_i^2(t)}{m_i(t)} + \frac{d_i(t)\dot{m}_i(t)}{m_i(t)}. \tag{25}$$

The proof of Theorem 1 can be found in [13].

Inequality (25) limits the rate of variation of the damping. It is noteworthy that this is a sufficient only condition, given by the particular choice of Lyapunov function in [55], which is always verified if the damping is incremented, but not when it is reduced. Since we plan the gains at discrete time intervals, we can approximate the stability condition (25) as

$$d_i(t+T) > d_i(t) - \frac{d_i^2(t)T}{m_i(t)} + \frac{d_i(t)\dot{m}_i(t)T}{m_i(t)}, \tag{26}$$

where T is the planner update period, i.e., sampling time. The terms $d_i(t+T)$ and $d_i(t)$ are respectively the newly planned damping (solution to (23)) and the current damping. In case (26) is satisfied, we can update the controller with the new damping value (23). Otherwise, to guarantee stability, we limit the damping variation as per (26). Note that $\dot{m}_i(t)$ needs to

be estimated online, but since the term $d_i(t)\dot{m}_i(t)T/m_i(t)$ is almost negligible (under Assumption 1), it can also be substituted by a worst case constant value.

A quick comment needs to be made on using the solutions $K = \mathrm{diag}(k_i)$ and $D = \mathrm{diag}(d_i)$ of (17) and (23), on the non-decoupled system (7). The off-diagonal terms in Λ couple the dynamics and make system (7) nonlinear. Using the diagonal approximation $\Lambda \approx \mathrm{diag}(m_i)$ is equivalent to linearizing the system about the equilibrium in the origin. For this reason, the approach presented in this section does not ensure global uniform asymptotic stability. However, asymptotic stability is still guaranteed and the effect of the off-diagonal terms is only to reduce the basin of attraction.

VI. CASE 2: NON-DIAGONALLY DOMINANT INERTIA

In the case in which the inertia Λ is not diagonally dominant, which might be the case, for instance, of a Cartesian impedance-controlled robotic arm, the method presented in Section V cannot be applied to solve optimization (11). A straightforward and blind approach to solve the problem would be to deal with optimization (14). This can be solved as such using state-of-the-art methods.

However, robust nonlinear optimization remains to date less studied than its linear counterpart [56], [57]. For this reason, hereafter, we present a better option to deal with (11): Section VI-A describes some preliminaries that lead to Section VI-B, where decoupling is forced in some new coordinates assuming a particular type of damping. This will allow us to replace the robust optimization with a deterministic one.

A. Preliminaries

Mechanical vibration theory (cf. [58]) shows that, if Λ is symmetric and positive definite, and D and K are symmetric and non-negative definite, the dynamics of (7) can be decoupled if and only if

$$D\Lambda^{-1}K = K\Lambda^{-1}D. \tag{27}$$

In this case, the matrix of generalized eigenvectors U of the undamped system, provided by

$$KU = \Lambda U\Gamma, \tag{28}$$

can be used to find new coordinates in which the system is decoupled [58]. In (28), Γ is a diagonal matrix containing the solutions γ_i of the corresponding generalized eigenvalue problem, given by

$$\det(K - \gamma_i\Lambda) = 0. \tag{29}$$

However, condition (27) is hardly applicable in practice since it leads to an additional nonlinear constraint. A more practical, sufficient condition for decoupling, which is also a particular case of (27), is

$$D = \alpha\Lambda + \beta K, \tag{30}$$

where α and β are real scalars. This condition forces the damping to be a linear combination of the inertia and the stiffness and is known in mechanical vibration theory as *proportional* damping.

Remark 3. Proportional damping *is to date one of the most commonly used damping models within linear analysis. It constrains and limits the oscillations to normal modes but presents some distinct advantages [59], the most important being the decoupling of the second order mechanical system.*

Assuming (30), equation (7) can be transformed into

$$\ddot{\mu} + (\alpha I + \beta\Gamma)\dot{\mu} + \Gamma\mu = \bar{U}^\intercal F_{\text{ext}} \quad (31)$$

by applying the coordinate change

$$\tilde{x} = \bar{U}\mu. \quad (32)$$

Here $\bar{U}$ is a mass-normalized version of U, i.e., $\bar{U}$ complies with

$$\bar{U}^\intercal\Lambda\bar{U} = I. \quad (33)$$

The steps leading from (7) to (31) can be found in [59].

Since Λ is always positive definite, equation (7) can be brought to the form in (31) only if the non-negative definiteness of the damping and the stiffness are assured [58].

Remark 4. *The non-negative definiteness of K and D is a necessary condition for the decoupling and stability of the closed-loop system.*

A symmetric non-negative definite matrix has a Cholesky decomposition: K can be factorized as

$$K = WW^\intercal, \quad (34)$$

where $W \in \mathcal{T}$, with $\mathcal{T}$ being the set of lower triangular matrices.

Remark 5. *Factorizing the stiffness matrix K as in (34) guarantees its non-negative definiteness and symmetricity. Additionally, if we constrain also α and β in (30) to be non-negative, also the damping matrix is ensured to be symmetric and non-negative definite. Hence, we satisfy the necessary condition for decoupling and stability.*

Taking into account (28), (29), and (33), and enforcing (30), (32), and (34), the robust optimization problem in (11) becomes

$$
\begin{aligned}
\underset{\alpha,\beta,W,\bar{U},\Gamma}{\arg\min} \quad & h(\alpha, \beta, W) \\
\text{s.t.} \quad & l_\alpha \leq \alpha \leq u_\alpha \\
& l_\beta \leq \beta \leq u_\beta \\
& l_{w_{i,j}} \leq w_{i,j} \leq u_{w_{i,j}} \\
& W \in \mathcal{T} \\
& \det(WW^\intercal - \gamma_i\Lambda) = 0 \\
& WW^\intercal\bar{U} = \Lambda\bar{U}\Gamma \\
& \bar{U}^\intercal\Lambda\bar{U} = I \\
\text{s.t.} \quad & \max_{\tilde{x}_0,\dot{\tilde{x}}_0} |\tilde{x}_i(t)| \leq b_i \quad \forall t \in [0, +\infty) \\
& \quad\quad l_{\tilde{x}_{0_i}} \leq \tilde{x}_{0_i} \leq u_{\tilde{x}_{0_i}} \\
\text{s.t.} \quad & \quad\quad l_{\dot{\tilde{x}}_{0_i}} \leq \dot{\tilde{x}}_{0_i} \leq u_{\dot{\tilde{x}}_{0_i}} \\
& \quad\quad \Lambda\ddot{\tilde{x}} + (\alpha\Lambda + \beta WW^\intercal)\dot{\tilde{x}} + WW^\intercal\tilde{x} = 0
\end{aligned}
$$
$$(35)$$

Here, the cost function to be minimized, the bounds and the constraints have been reconsidered in function of α, β and W, since we imposed $D = \alpha\Lambda + \beta K$ and $K = WW^\intercal$.

Remark 6. *The set $\mathcal{T}$ of lower triangular matrices is convex. Given a generic matrix $A \in \mathbb{R}^{n \times n}$, its orthogonal projection onto $\mathcal{T}$ is trivial since it involves zeroing the elements above the diagonal of A through an operator* $\text{tril}(\cdot)$:

$$\text{Proj}_{\mathcal{T}}(A) = \text{tril}(A).$$

Projected optimization methods can efficiently deal with the constraint $W \in \mathcal{T}$.

The advantage of (35) is that the constraint

$$\Lambda\ddot{\tilde{x}} + (\alpha\Lambda + \beta WW^\intercal)\dot{\tilde{x}} + WW^\intercal\tilde{x} = 0, \quad (36)$$

together with (28), (29), (30), (32), (33), and (34), expressed in the coordinates μ (modal coordinates), leads to the homogeneous part of (31), which is a set of six decoupled second order differential equations. Hence, we would be forcing the decoupling of the closed-loop system in the modal coordinates.

If we choose a convex objective function $h(\alpha, \beta, W)$ for minimizing the impedance, the constrained robust optimization problem (35) is convex in all components except for constraints (28), (29) and (33), which are non-convex and respectively bilinear, polynomial and quadratic. The constraint on the peak keeps the complexity of the optimization high.

In the following, (35) is transformed into the modal coordinates. The resulting problem will have the advantage that the robust optimization problem is made deterministic.

B. Decoupled Optimization

In modal coordinates, applying (32), equation (36) turns out to be decoupled into p single degree of freedom systems:

$$\ddot{\mu}_i + \underbrace{(\alpha + \beta\gamma_i)}_{a_1}\dot{\mu}_i + \underbrace{\gamma_i}_{a_0}\mu_i = 0. \quad (37)$$

An analytical solution to the maximum of $\mu_i(t)$ can be found. Re-writing (35) in modal coordinates yields

$$
\begin{aligned}
\underset{\alpha,\beta,W,\bar{U},\Gamma}{\arg\min} \quad & h(\alpha, \beta, W) \\
\text{s.t.} \quad & l_\alpha \leq \alpha \leq u_\alpha \\
& l_\beta \leq \beta \leq u_\beta \\
& l_{w_{i,j}} \leq w_{i,j} \leq u_{w_{i,j}} \\
& W \in \mathcal{T} \\
& \det(WW^\intercal - \gamma_i\Lambda) = 0 \\
& WW^\intercal\bar{U} = \Lambda\bar{U}\Gamma \\
& \bar{U}^\intercal\Lambda\bar{U} = I \\
\text{s.t.} \quad & \max_{\mu_{i_0},\dot{\mu}_{i_0}} |\mu_i(t)| \leq b_{\mu_i} \quad \forall t \in [0, +\infty) \\
& \quad\quad l_{\mu_{0_i}} \leq \mu_{0_i} \leq u_{\mu_{0_i}} \\
\text{s.t.} \quad & \quad\quad l_{\dot{\mu}_{0_i}} \leq \dot{\mu}_{0_i} \leq u_{\dot{\mu}_{0_i}} \\
& \quad\quad \ddot{\mu}_i + a_1\dot{\mu}_i + a_0\mu_i = 0.
\end{aligned}
$$
$$(38)$$

Here, recalling that for the generalized eigenvalue problem it generally holds that $\bar{U}^{-1} \neq \bar{U}^\intercal$, the whole maximization constraint has been transformed into the new coordinates.

$$
\begin{aligned}
l_{\mu_{0_i}} &= \bar{U}^{-1}l_{\tilde{x}_{0_i}}; \quad u_{\mu_{0_i}} = \bar{U}^{-1}u_{\tilde{x}_{0_i}}; \\
l_{\dot{\mu}_{0_i}} &= \bar{U}^{-1}l_{\dot{\tilde{x}}_{0_i}}; \quad u_{\dot{\mu}_{0_i}} = \bar{U}^{-1}u_{\dot{\tilde{x}}_{0_i}}; \\
b_{\mu_i} &= \bar{U}^{-1}b_i.
\end{aligned}
$$

In (38), α, β, and W being fixed, the robust maximization can be replaced by p nonlinear inequality constraints.

To show this, observe the following. The p maximization constraints of (38) impose to comply with the bounds b_{μ_i} at each instant for unknown but bounded initial conditions μ_{i_0} and $\dot{\mu}_{i_0}$. Hence, similarly to [13] and Section V, we focus on the worst case and consider, without loss of generality, $\mu_{i_0} > 0$ and $\dot{\mu}_{i_0} > 0$. As a matter of fact, the absolute value on $\mu_i(t)$ can be removed since the peak would be positive. Moreover, re-adjusting the bounds as $\mu_{0_i,\max} \triangleq \max(|l_{\mu_{0_i}}|, u_{\mu_{0_i}})$ and $\dot{\mu}_{0_i,\max} \triangleq \max(|l_{\dot{\mu}_{0_i}}|, u_{\dot{\mu}_{0_i}})$, each maximization constraint in (38) can be re-written as

$$
\begin{aligned}
\max_{\mu_{i_0}, \dot{\mu}_{i_0}, t} \quad & \mu_i(t) \leq b_{\mu_i} \\
\text{s.t.} \quad & t \geq 0. \\
& 0 \leq \mu_{0_i} \leq \mu_{0_i,\max} \\
& 0 \leq \dot{\mu}_{0_i} \leq \dot{\mu}_{0_i,\max} \\
& \ddot{\mu}_i + a_1 \dot{\mu}_i + a_0 \mu_i = 0.
\end{aligned} \tag{39}
$$

Following the steps in Appendix B, an upper bound f_{c_i} on the peak of $\mu_i(t)$ can be found (cf. (57)) for the worst-case initial conditions $\mu_{0_i,\max}$ and $\dot{\mu}_{0_i,\max}$ and for a specific oscillatory behaviour (for instance, over-damped). By imposing this upper bound to be below b_{μ_i}, (38) can be modified into

$$
\begin{aligned}
\arg\min_{\alpha, \beta, W, \bar{U}, \Gamma} \quad & h(\alpha, \beta, W) \\
\text{s.t.} \quad & l_\alpha \leq \alpha \leq u_\alpha \\
& l_\beta \leq \beta \leq u_\beta \\
& l_{w_{i,j}} \leq w_{i,j} \leq u_{w_{i,j}} \\
& W \in \mathcal{T} \\
& \det(WW^\intercal - \gamma_i \Lambda) = 0 \\
& WW^\intercal \bar{U} = \Lambda \bar{U} \Gamma \\
& \bar{U}^\intercal \Lambda \bar{U} = I \\
& \chi_i(\alpha, \beta, \Gamma) > 1 \\
& f_{c_i}(\mu_{0_i,\max}, \dot{\mu}_{0_i,\max}, \alpha, \beta, W) \leq b_{\mu_i}.
\end{aligned} \tag{40}
$$

Here, as mentioned before, the last inequality replaced the maximization constraint. The additional constraint on the damping ratio χ_i, used for ensuring an over-damped behavior of the ith closed-loop subsystem (37), is nonlinear.

Minimization problem (40) is deterministic and, thus, much simpler than (35). There is a very wide literature on deterministic optimizations involving the types of constraint functions in (40); see, for example, [60], [61], [62] and [63]. Even though global optimization of such non-convex problems is time-consuming and cannot be achieved in real-time, numerical methods can efficiently address them utilizing branch-and-bound, cutting, and approximation algorithms; for instance, [64] and [65] present two Reformulation-Linearization Techniques that lead to linear programming problems, which in turn produce tight lower bounds on the solution of the original bilinear and polynomial problems. Some efficient algorithms for nonlinear programming include the Interior Point Method [66] and some others found in [67].

It behoves us to point out that it is not conceivable to guarantee *a priori* that nonlinear programs, such as (40), always lead to non-empty solution space [68]. However,

experiments performed on a state-of-the-art robot show that, in practice, numerical solutions to (40) are always found (see Section VIII). This is reasonable since, as long as the maximum allowed initial perturbation $\tilde{x}_{0_i,\max}$ is within the bounds b_i, it is theoretically always possible to find controller gains to limit the relative peak to arbitrarily small values. Moreover, in the very unlikely case that no solution is found, we forward to the controller the solution found at the previous iteration, adequately modified to ensure stability of the origin and passivity of the closed-loop system.

C. Stability and Passivity Analysis

Optimization (35), or equivalently (40), produces, at the nth iteration, a solution, i.e., a stiffness $K_n = W_n W_n^\intercal$ and a damping $D_n = \alpha_n \Lambda_n + \beta_n W_n W_n^\intercal$. The actual gains of the impedance controller should be updated, only after ensuring the stability of the origin and the passivity of the closed-loop system (7).

Given the second order linear time-varying system

$$
\Lambda(t)\ddot{\tilde{x}} + D(t)\dot{\tilde{x}} + K(t)\tilde{x} = F_{\text{ext}}, \tag{41}
$$

its stability and passivity properties can be studied using the analyses presented in [12] and [28]. We re-write (41) as

$$
\ddot{\tilde{x}} + \underbrace{\Lambda^{-1}(t)D(t)}_{D'(t)} \dot{\tilde{x}} + \underbrace{\Lambda^{-1}(t)K(t)}_{K'(t)} \tilde{x} = \bar{F}_{\text{ext}}. \tag{42}
$$

We define two operators $\bar{\lambda}(\cdot)$ and $\underline{\lambda}(\cdot)$ that extract the largest and smallest eigenvalues from their arguments.

Theorem 2. *Let $D'(t)$ and $K'(t)$ be symmetric, positive definite and continuously differentiable matrices $\forall t \geq 0$, the origin of (41) is globally uniformly asymptotically stable (for $F_{\text{ext}} = 0$) and (41) is a passive map from F_{ext} to $\dot{\tilde{x}} + \delta_t \tilde{x}$ if $Y(t) = \dot{K}'(t) + \delta_t \dot{D}'(t) - 2\delta_t K'(t)$ is negative definite (n.d.) for $\delta_t = \min_t \underline{\lambda}(D'(t))$.*

The proof of Theorem 2 follows directly from Theorem 1 in [12] and equations (12)-(13) in [28].

Remark 7. *Equation (42) assumes $\Lambda(t)$ positive definite. This always holds except in pathological situations, e.g., kinematic singularity. This brings back the requirement of positive definiteness of $D'(t)$ and $K'(t)$ to that of $D(t)$ and $K(t)$.*

Remark 8. *Theorem 2 provides a sufficient only condition to ensure the uniform asymptotic stability of the origin and the passivity of (7) [12], [28]. It might be possible to find less conservative conditions for other choices of Lyapunov candidate and storage function.*

Theorem 2 can be re-formulated in relation to the discrete-time solutions of the optimization as follows.

Given a newly planned impedance (Λ_n, D_n, K_n) (n^{th} planning iteration with optimization (35)) and the previous step solution $(\Lambda_{n-1}, D_{n-1}, K_{n-1})$, assuming the planning period T to be relatively small, the newly computed impedance does not compromise the stability of the origin and the passivity of (7) if the following is verified at each iteration:

Condition 1.

$$Y_d = \frac{(K'_n - K'_{n-1})}{T} + \delta\frac{(D'_n - D'_{n-1})}{T} - 2\delta K'_n$$

is n.d. for $\delta = \min_j \underline{\lambda}(D'_j)$ *and* $j \in \{0, \cdots, n-1\}$.

If Condition 1 is not satisfied, we might want to modify K_n or D_n so that stability/passivity is ensured. To this end, we introduce two scaling factors $c_{K_n}, c_{D_n} > 0$ to scale the variations Δ_{K_n} and Δ_{D_n}.

$$K^\star_n = K_{n-1} + c_{K_n}\Delta_{K_n}; \quad \Delta_{K_n} = K_n - K_{n-1}.$$
$$D^\star_n = D_{n-1} + c_{D_n}\Delta_{D_n}; \quad \Delta_{D_n} = D_n - D_{n-1}.$$

We substitute these in Condition 1 to compute the c_{K_n} and c_{D_n} that guarantee a stable and passive closed-loop system. We apply triangle inequalities on the largest eigenvalue of the modified Y_d.

$$\bar{\lambda}(Y^\star_d) \leq \bar{\lambda}(\frac{1}{T}c_{K_n}\Delta_{K_n} + \frac{\delta}{T}\delta c_{D_n}\Delta_{D_n} \tag{43}$$
$$- 2\delta\left[K'_{n-1} + c_{K_n}\Delta_{K_n}\right])$$
$$\leq \frac{c_{K_n}}{T}\bar{\lambda}(\Delta_{K_n}) + \frac{c_{D_n}\delta}{T}\bar{\lambda}(\Delta_{D_n}) \tag{44}$$
$$- 2\delta\underline{\lambda}(K'_{n-1}) - 2c_{K_n}\delta\underline{\lambda}(\Delta_{K_n}).$$

If Condition 1 is not met, to render the error dynamics stable and the closed-loop system passive, the variations of the stiffness Δ_{K_n} and damping Δ_{D_n} can be scaled respectively of factors c_{K_n} and c_{D_n} that comply with

Condition 2.

$$\frac{c_{K_n}}{T}\bar{\lambda}(\Delta_{K_n}) + \frac{c_{D_n}\delta}{T}\bar{\lambda}(\Delta_{D_n}) - 2\delta\Theta \leq 0,$$

with $\Theta = \underline{\lambda}(K'_{n-1}) + c_{K_n}\underline{\lambda}(\Delta_{K_n})$.

Notice that the unknowns of the single inequality in Condition 2 are c_{K_n} and c_{D_n}. It should be noted that guaranteeing stability/passivity can undermine the observance of the *performance requirement*. Indeed, small scaling factors might make it impossible to comply with the maximization constraint in (39). It is not possible to guarantee that both the stability/passivity and the *performance requirement* are always met using the proposed method. If the solution provided by optimization (40) does not comply with Condition 1, we limit ourselves to ensure only the stability/passivity using Condition 2.

VII. IMPEDANCE PLANNING

In this section, we outline our general algorithm. It chooses one of the two methods, presented in Sections V and VI, for computing the optimal impedance for the cases of diagonally dominant and non-diagonally dominant inertia.

According to the inertia Λ, either optimization (16) or (40) are solved in a loop with a period T in combination with the respective methods for guaranteeing stability/passivity, shown in Sections V-B and VI-C. In the case of diagonally dominant inertia, the closed-form solution provided by (23) is directly employed and (26) is utilized to ensure stability. On the contrary, if the closed-loop system has a non-diagonally dominant inertia, (40) is solved by using state-of-the-art numerical

methods (e.g., the Interior Point Method [66]). Condition 2 ensures stability/passivity.

Algorithm 1 Optimal Impedance Planning

Input: $\mathcal{S}, T$
Output: $K_{\text{out}}, D_{\text{out}}$
  $(K_0, D_0) \leftarrow InitializeImpedance(\mathcal{S})$
  repeat
    $\mathcal{S} \leftarrow GetBounds()$
    $\Lambda_n \leftarrow GetMassMatrix()$
    $(K_n, D_n) \leftarrow SolveOptimization(\Lambda_n, \mathcal{S})$
    if $Stability/PassivityCheck(\Lambda_n, K_n, D_n)$ **then**
      $(K_{\text{out}}, D_{\text{out}}) \leftarrow OutputGains(K_n, D_n)$
    else
      $(K^\star_n, D^\star_n)$
        $\leftarrow EnforceStability/Passivity(\Lambda_n, K_n, D_n, \mathcal{S})$
      $(K_{\text{out}}, D_{\text{out}}) \leftarrow OutputGains(K^\star_n, D^\star_n)$
    end if
    $WaitForPeriod(T)$
  until $StoppingCondition$

The basic structure of the optimal impedance planner is shown in Algorithm 1. It requires two inputs: (i) the set $\mathcal{S} = \{l_{k_{i,j}}, u_{k_{i,j}}, l_{d_{i,j}}, u_{d_{i,j}}, l_{\tilde{x}_{0_i}}, u_{\tilde{x}_{0_i}}, l_{\dot{\tilde{x}}_{0_i}}, u_{\dot{\tilde{x}}_{0_i}}, b_i\}$ of bounds on the stiffness and damping, on the initial conditions, and on the peak of the Cartesian error and (ii) the planner period T.

Initially, two matrices K_0 and D_0, which ensure compliance with the *performance requirement*, are initialized by the function $InitializeImpedance$. At this point the planner repeats in a loop with period T the following:

1) The bounds in $\mathcal{S}$ are updated by $GetBounds$ if any new ones are specified by a higher-level task planner.
2) The current Cartesian mass matrix Λ_n is read using the function $GetMassMatrix$.
3) For the read inertia, according to its diagonal dominance, the function $SolveOptimization$ finds optimal impedance (K_n, D_n) solving either (16), using (23) and (17), or (35) by means of numerical methods on (40).
4) Using equation (26) or Condition 1, based on Λ_n, $Stability/PassivityCheck$ returns true if the update of the controller gains with the new ones is guaranteed to preserve stability/passivity. Else, it returns false.
5) If stability/passivity are not compromised, closed-loop impedance is updated by $OutputGains$.
6) Else, the function $EnforceStability/Passivity$ utilizes either the boundary of (26) as the new damping or Condition 2 to restore stability/passivity. Also this step is performed based on whether Λ_n is diagonally dominant.
7) Then, the new stiffness $K^\star_n$ and damping $D^\star_n$ are used to update the controller gains.
8) Finally, the planner waits for the completion of the planning period T.

The choice of the planning period T should be a trade-off between small T, to have a precise estimate of the derivatives of the impedance gains for guaranteeing stability/passivity, and high T for ensuring the convergence of the optimizations in Algorithm 1. The set $\mathcal{S}$ is provided by a higher level reasoning

Table I
PARAMETERS USED FOR EXPERIMENTAL VALIDATION

Validation	Parameter	Unit	Value‡	Parameter	Unit	Value‡
ANYmal B with [19] and [13]	$b_i^{(1)}$	m	{0.06, 0.055, 0.05}	$b_i^{(2)}$	m	{0.02, 0.02, 0.02}
	$\tilde{x}_{0_i,\max}$	m	{0.034, 0.036, 0.019}	$\dot{\tilde{x}}_{0_i,\max}$	m/s	{0.216, 0.181, 0.126}
	l_{k_i}	N/m	{300, 300, 300}	u_{k_i}	N/m	{1800, 1800, 1800}
	l_{d_i}	Ns/m	{230, 230, 230}	u_{d_i}	Ns/m	{450, 450, 450}
	K_{low}	N/m	diag([500, 500, 500])	K_{high}	N/m	diag([1500, 1500, 1500])
	D_{low}	Ns/m	diag([90, 90, 90])	D_{high}	Ns/m	diag([200, 200, 200])
Franka Emika Panda with [10] or [69] and *Standard Method* or *Algorithm 1*	$b_i^{(1)}$	m	{0.03, 0.03, 0.03}	$b_i^{(2)}$	m	{0.036, 0.036, 0.036}
	$\tilde{x}_{0_i,\max}$	m	{0.025, 0.025, 0.025}	$\dot{\tilde{x}}_{0_i,\max}$	m/s	{0.03, 0.03, 0.03}
	$l_{k_{i,j}}$	N/m	{150, 5, 5, 150, 5, 150}*	$u_{k_{i,j}}$	N/m	{390, 50, 50, 390, 50, 390}*
	$l_{d_{i,j}}$	Ns/m	{1280, 460, 460, -30, 1990, -880, 1350}*	$u_{d_{i,j}}$	Ns/m	{5035, 2000, 330, 4800, 5500, 3300}*
	K_{low}	N/m	diag([150, 150, 150])	K_{high}	N/m	diag([390, 390, 390])
	D_{low}	Ns/m	diag([24.5, 24.5, 24.5])	D_{high}	Ns/m	diag([39.5, 39.5, 39.5])

* Elements of the vectorization of the lower triangular blocks of matrices $K_{\min}$, $K_{\max}$, $D_{\min}$, and $D_{\max}$, respectively. See Appendix C.

‡ For the sake of conciseness, we show only the values of the components of each parameter related to translation, i.e., $\tilde{x}_1$, $\tilde{x}_2$, and $\tilde{x}_3$.

or task planner, which, for instance, can change the bounds based on the robot model, on the information provided by a vision system and on the required precision for the task being performed by the robot. An example of strategy that the higher level planner can adopt for the choice of the set $\mathcal{S}$ is provided in Appendix C.

An observation is due on why we do not always use the approach presented in Section VI. The main reason is the advantage provided by the closed form solution (23). Hence, whenever the inertia is diagonally dominant, the method of Section V is to be preferred since it provides a faster solution, which is valid for small tracking errors. Instead, solving optimization (40) in the case of non-diagonally dominant inertia might be more time consuming depending on the particular numerical optimization tool (and its implementation), but the solution is more precise than (23) and globally valid.

VIII. EXPERIMENTAL VALIDATION

We validate the proposed impedance planner (Algorithm 1) on two different robots: the quadruped ANYmal B [3] and the 7 DoF robotic arm Franka Emika Panda [70]. We modulate the impedance of the torso of ANYmal using the controller in [19]. The Panda robot is controlled using the non inertia shaping Cartesian impedance controller provided by Franka Emika (similar to the one presented in [69]), which has been modified only to receive varying stiffness and damping matrices. We also implemented an inertia shaping impedance controller, based on [10]. To this end, we used an ATI Mini45 6-axis force/torque sensor [71] since the external force measurements provided by the robot were too noisy to be fed back to the controller (see again Section II-A). We mounted a soft gripper [72] developed by QB Robotics for grasping objects. The three impedance controllers run on ROS at an average rate of ≈ 400 Hz for ANYmal and ≈ 850 Hz for the Panda. To solve optimization (40), used in Algorithm 1, we used the interior-
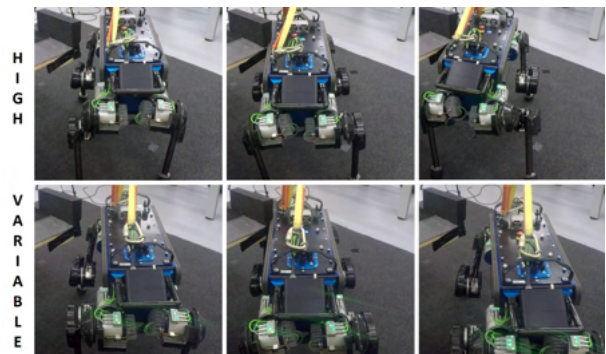

Figure 4. Experiments on ANYmal. ANYmal colliding with an unperceived obstacle. A fixed high impedance produces high contact forces that trigger the emergency stop. Variable impedance, instead, increases robot compliance to withstand the disturbance.

point method provided by MATLAB. The main parameters used for validation are reported in Table I.

A. Case: Diagonally Dominant Inertia

Since the closed-loop inertia of the torso of ANYmal is diagonally-dominant, Algorithm 1 chooses the method proposed in Section V. A planning period $T = 0.0025$ s is used. We set the parameters $\tilde{x}_{0_i,\max}$ and $\dot{\tilde{x}}_{0_i,\max}$ as in Table I. These are the maximum position and velocity errors that we measured while walking the real robot on an uneven terrain with the fixed gains employed in [19]. The diagonal impedance limits l_{k_i}, u_{k_i}, l_{d_i}, and u_{d_i} are also reported in Table I.

1) Identification Procedure: Initially, we found a mismatch between the simulated and the real closed loop dynamics. This was caused by inaccuracies in the dynamic model used by the impedance controller. In particular, the translational damping of the system was much different from the expected one.

Hence, we estimated the intrinsic translational damping and mass of the system using a least squares approach. After zeroing the damping gain, for several stiff-
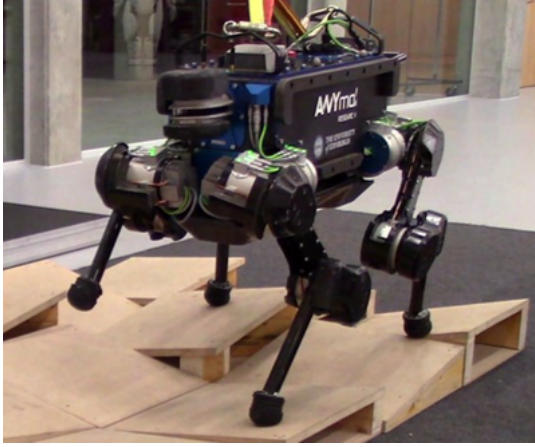
Figure 5. Experiments on ANYmal. ANYmal engaging rough terrain aided by our impedance planning algorithm.

ness gains we applied the following displacements to the robot: $\tilde{x}_0 = \{10, \ 20, \ 35, \ 50\}$ mm along the x axis, $\tilde{x}_0 = \{10, \ 20, \ 35, \ 50\}$ mm along the y axis and $\tilde{x}_0 = \{50, \ 100, \ 150, \ 170\}$ mm along the z axis. For each of the tested stiffness values, we applied the displacements for three times. The stiffness values we used are $k = 800$ N/m, $k = 1000$ N/m and $k = 1200$ N/m.

The identification process resulted in $\tilde{d}_x = 50.4885$ Ns/m, $\tilde{d}_y = 64.4859$ Ns/m and $\tilde{d}_z = 75.6533$ Ns/m, while $\tilde{m}_x$, $\tilde{m}_y$ and $\tilde{m}_z$ were found to be approximately equal to the diagonal elements of the matrix Λ in the default configuration. These identified damping values were used as an offset to the optimal ones (23) in Algorithm 1.

2) Obstacle Interaction Experiment: In the first experiment, we walk the robot along a path where it touches an obstacle placed at approximately 0.6 m of height from the ground. We perform the same test using fixed-low (K_{low}, D_{low}), fixed-high (K_{high}, D_{high}), and Algorithm 1 using boundaries $b_i^{(1)}$. The values of these parameters are reported in Table I. The fixed impedance values are the same as in [19]. In Figure 4, we show some photo-sequences for the cases of high and variable impedance. The low impedance case had similar behavior to the variable gains' scenario. In the case of high impedance, as expected, a large interaction force causes the robot to stop. On the contrary, by varying the impedance using our planner, the robot withstands the reduced force exerted by the environment. This clearly shows the benefit of our approach.

3) Rough Terrain Experiment: In the second experiment, we walk ANYmal on rough terrain (see Figure 5). We use the locomotion planner proposed in [73]. The terrain consists of randomly combined wooden tiles (approximately 0.4×0.4m) with different inclinations ($\{\pi/36, \ \pi/18, \ \pi/12\}$rad).

Towards the middle of the path, we change the task requirements from $b_i^{(1)}$ to $b_i^{(2)}$ (see Table I) and then we reset them to the initial values. The tracking error and the varying impedance are reported in Figure 6. The unevenness of the terrain and the changes in the support polygon are taken into account by the impedance planner, which causes variations of the impedance gains. This allows achieving the desired tracking performance and, hence, to keep balance. The values of the tracking error stay always within the specified

boundaries even when the b_i are tightened in the time interval from $t = 38$ s to $t = 53$ s. Notice also that, due to the offset explained in Section VIII-A1, the damping coefficients reach also values smaller than l_{d_i}.

B. Case: Non-diagonally Dominant Inertia

The Cartesian inertia (without inertia shaping) of the Panda robot is non-diagonally dominant. Hence, Algorithm 1 chooses the method proposed in Section VI to plan the impedance. A planning period $T = 0.03$ s is used. The planner input parameters are reported in Table I. We set the parameters $l_{\tilde{x}_{0_i}} = -\tilde{x}_{0_i,\max}$, $u_{\tilde{x}_{0_i}} = \tilde{x}_{0_i,\max}$ and $l_{\dot{\tilde{x}}_{0_i}} = -\dot{\tilde{x}}_{0_i,\max}$, and $u_{\dot{\tilde{x}}_{0_i}} = \dot{\tilde{x}}_{0_i,\max}$. The impedance limits $l_{k_{i,j}}$, $u_{k_{i,j}}$, $l_{d_{i,j}}$, and $u_{d_{i,j}}$ are also reported. Please refer to Appendix C for a possible method to compute the input set $\mathcal{S}$ of our planner.

For a fair evaluation, we perform two sets of experiments: the first with the inertia shaping controller, which gives us a baseline for comparison, and the second with the non inertia shaping controller. Each set consists of three tests with different choices of impedance: 1) fixed-low impedance, 2) fixed-high impedance, and 3) variable impedance.

In this last case, according to the controller, we use either Algorithm 1 or the method in [12] to guarantee stability while switching between high and low impedance (which are the same used for the fixed impedance cases). We call this latter approach *Standard Method*. We wish to stress that the *Standard Method*, which switches between fixed gains for complying with requirements on the tracking error and compliance, requires closed-loop decoupling through inertia shaping in order to apply established single DoF techniques.

For both sets of experiments, the fixed gains are chosen to be diagonal: the low and high stiffness matrices, K_{low} and K_{high}, contain the diagonal elements respectively of $K_{\min}$ and $K_{\max}$ from Appendix C. The dampings D_{low} and D_{high} are chosen to ensure a critically damped behavior.

We introduce three metrics for quantitative performance evaluation. These are

$$\mathcal{M}_{\tilde{x}} = \sum_i \int_{t_0}^{t_f} ReLU(|\tilde{x}_i| - b_i)\, dt, \tag{45}$$

for the compliance of tracking error $\tilde{x}$ with its bound b,

$$\mathcal{M}_{F_{\text{ext}}} = \sum_i \int_{t_0}^{t_f} |F_{\text{ext},i}|\, dt, \tag{46}$$

measuring the minimization of the contact force, and

$$\mathcal{M}_{\tau} = \sum_i \int_{t_0}^{t_f} |\tau_i|\, dt, \tag{47}$$

measuring the minimization of the control torque. The lower the value of these $\mathcal{M}_{(\cdot)}$ in the time interval $[t_0, t_f]$, the better the performance of the corresponding gain choosing method.

We also use an additional binary metric $\mathcal{M}_{\text{task}}$ related to the correct execution of the task.

$$\mathcal{M}_{\text{task}} = \begin{cases} 0, & \text{if task failed,} \\ 1, & \text{if task success.} \end{cases} \tag{48}$$

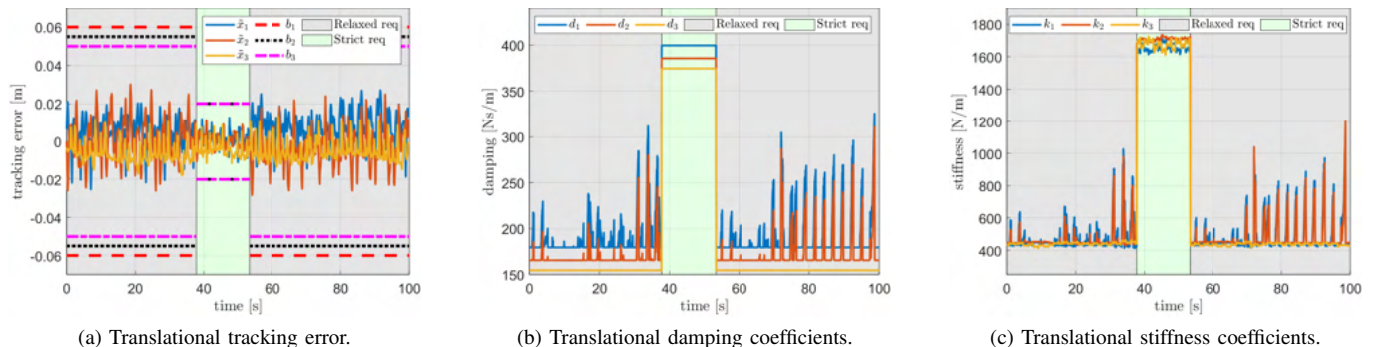(a) Translational tracking error. (b) Translational damping coefficients. (c) Translational stiffness coefficients.

Figure 6. Experiment with ANYmal on rough terrain. (a) The margins b_i are tightened at $t = 38$s and later reset at $t = 53$s. The tracking error is always maintained within the boundaries. (b,c) Algorithm 1 automatically computes impedance gains.

A photo of the experimental setup and the manipulated objects is provided in Figure 7. The *manipulandum* is a piece of wood that has the shape of a rectangular cuboid and weighs approximately 0.15 kg. The desired Cartesian trajectory of the gripper consists of an *approach* phase towards the grasp pose (red cross), a *post-grasp* phase, in which the grasped object is lifted, a *moving* phase, where the robot moves to the other end of the table with the object grasped, and, finally, the *release* phase, when the object is released in a target location (green tick). We place three heavy cans of pickle as obstacles in such a way that, while tracking ideally the desired trajectory, the robot end-effector collides with all three cans.

The choice of this particular setup is motivated by its simplicity, which favors reproducibility and repeatability. These are critical for comparing the different approaches in the same conditions. Additionally, with this setup, we emulate a worst-case scenario, in which motion planning and sensing capabilities are weakened. This highlights the actual benefits provided by the controller and the choice of the impedance.

Photo sequences of the two sets of three experiments are shown in Figures 8 and 9, respectively, for the cases of inertia shaping and no inertia shaping. Results are shown in Figures 10 and 11 through plots of the controller gains, the external force, the tracking errors, and the control torques. For the sake of space, we do not show the plots of orientation tracking errors, which had similar behavior to the translational ones. We also do not show the tracking error along $\tilde{x}_3$, since interactions mostly happen in the other two directions.

The values of the metrics are reported in Table II. Please,

Figure 7. The experimental setup for the case of non-diagonally dominant inertia. A Franka Emika Panda robot mounts an ATI Mini45 force/torque sensor and a QB SoftClaw gripper. The object (■) should be grasped and transported from the initial (✗) to the goal (✓) position.

see also the video attached to this submission. In the following, we discuss the results and present relevant insights categorized based on the choice of impedance.

1) Fixed Low Impedance: Here, we discuss the results of the two tests using fixed-low stiffness K_{low} and damping D_{low} (see Table I). The blue lines in Figures 10 and 11 show the evolution of the relevant quantities for the inertia shaping and non inertia shaping cases, respectively.

In both cases, the task is failed because of the reduced precision. This is because low impedance does not compensate for model uncertainties in the controllers. Indeed, the object is not grasped (see submitted video). However, the trajectory is tracked till the end despite the collisions with the obstacles since interaction forces are not high. Because of the decoupling performed by inertia shaping, Figures 10d and 10e display smaller tracking errors than in Figures 11d and 11e. Also, notice how the interaction forces are surprisingly very high (see blue lines in Figures 10c and 11c, and Table II): this is caused by the high tracking errors accumulated from the beginning of the task leading, in turn, to deeper interactions.

2) Fixed High Impedance: Here, we discuss the fixed-high impedance experiments with the two controllers. We employ stiffness K_{high} and damping D_{high} (see Table I). The relevant quantities are plotted in yellow in Figures 10 and 11.

Both experiments display smaller tracking errors, which is reasonable since high controller gains compensate for model uncertainties and improve tracking. Nevertheless, a stiffer robot leads to higher contact forces during unforeseen collisions. This is what happens at $t \approx 33$ s (yellow line in Figures 10c and 11c). It is worth mentioning that, due to coupling, slightly higher external forces are generated in the case of avoidance of inertia shaping, triggering the safety stop of the Panda robot and causing task failure.

3) Variable Impedance (Standard Method / Algorithm 1): In the following, we discuss experiments using the *Standard Method* and compare it with the proposed impedance planner.

The red lines in Figures 10 and 11 show the evolution of the relevant quantities for the two cases. Notice how, while the *Standard Method* acts directly by changing the gains with no guarantees on the *performance requirements*, Algorithm 1 automatically tunes the gains taking into account changes in the bounds on the tracking error. Indeed, the b_i are relaxed from $b_i^{(1)}$ to $b_i^{(2)}$ during the *moving* phase, in which impacts are

Table II
EXPERIMENTAL RESULTS AND OBSERVATIONS

Impedance Controller	Impedance Planner	$\mathcal{M}_{\tilde{x}}$	$\mathcal{M}_{F_{\text{ext}}}$	$\mathcal{M}_\tau$	$\mathcal{M}_{\text{task}}$	Observations			
						F/T Sensor	Precision	Ext. Forces	Control Torques
Inertia Shaping ([10])	Fixed Low	4.22	5.18e3	6.61e3	✗	Required	Low	Low	High
	Fixed High	1.67	5.70e3	7.26e3	✓	Required	High	High	High
	Standard Method	0.35	5.27e3	6.81e3	✓	Required	High	Low	High
No Inertia Shaping ([69])	Fixed Low	1.25	5.63e3	3.42e3	✗	Not Required	Low	Low	Low
	Fixed High	19.76§	1.16e4§	4.19e3	✗	Not Required	High	High	Low
	Algorithm 1	0.65	5.70e3	3.53e3	✓	Not Required	High	Low	Low

§ High values of $\mathcal{M}_{\tilde{x}}$ and $\mathcal{M}_{F_{\text{ext}}}$ attributable to task failure resulting from the trigger of robot safety stop. See Figure 9b and the yellow line in Figure 11c.

foreseen and precision can be reduced. In case of Algorithm 1, impedance gains are varied both within the same phase due to the changes in robot configuration, and across two phases because of the variation of the bounds. Tighter bounds produce higher impedance values, while loosening the bounds results in lower stiffness and damping computed by the impedance planner. Notice, in both cases, the smooth variations of the impedance caused by guaranteeing stability/passivity (see Section VI-C and [12]). We also note that, during the experiments, optimization (40) always converged to a feasible solution.

Additionally, recall Remark 1: since, in our setup, the properties of the object are known, the controllers compensate for the constant load lifted by the gripper. However, if the load were unknown, another practical and viable solution enabled by Algorithm 1 would be to tighten the bounds b_i during the *post-grasp* and *moving* phases. This would generate slightly higher impedance gains that counterbalance the model uncertainty introduced by the constant load.

For both the variable impedance cases, results show better tracking performance with respect to the corresponding low impedance cases, as the red lines in Figures 10d and 10e, and Figures 11d and 11e clearly indicate. The specified bounds are observed except for the brief instants of time in which the manipulator falls behind the planned trajectory as it is colliding compliantly with the obstacles with non ideal impulsive contact forces. Here, notice also how the forces in Figures 10c and 11c have dynamics much slower than reaction time of the control-loop (≈ 1 ms for the Franka Emika). Hence, impedance control will be able to properly set the desired behavior.

In both the tests, the manipulation task is successfully completed. Indeed, the robot never triggers a safety stop because the measured external forces are kept low. Higher accuracy in tracking the references w.r.t. the low gains case and lower impedance w.r.t. the fixed high impedance case produce smaller contact forces (red lines in Figures 10c and 11c).

The evaluation clearly demonstrates the advantages of variable impedance. Some additional experiments on a slightly different setup, using the non inertia shaping controller, are also shown in the submission video: these provide further support to our claims.

An additional insight emerging from the experiments is that using fixed impedance does not always guarantee consistent results: notwithstanding compliance, low impedance can produce high contact forces due to increased tracking errors; high gains can produce task failures, despite increased precision, due to strong impacts.

Finally, the proposed planner is shown to be comparable in terms of performance to a standard impedance varying method using inertia shaping. More in detail, our method compares to the *Standard Method* as follows (cf. Table II):

1) The *Standard Method* has better tracking performance $\mathcal{M}_{\tilde{x}}$ thanks to the decoupling of the inertia. Algorithm 1 achieves comparable performance despite avoiding inertia shaping.
2) Decoupling reduces the external forces (see $\mathcal{M}_{F_{\text{ext}}}$) during impacts in the case of the *Standard Method*, while coupled inertia causes slightly higher contact forces when using Algorithm 1.
3) The feedback of external forces leads to higher values of control torques (confirmed by $\mathcal{M}_\tau$) for the *Standard Method*, despite smaller tracking errors. Algorithm 1 keeps the control low by avoiding inertia shaping.
4) The *Standard Method* demands the use of precise (and often costly) force/torque sensors for performing the required inertia shaping. Our Algorithm does not require costly sensors since no inertia shaping is required.

These observations are also summarized in the last column block of Table II.

By autonomously choosing the minimum closed-loop impedance that ensures compliance with some provided *performance requirement*, Algorithm 1 attacks the hindrance of coupled inertia and reduces the entity of unexpected impacts while assuring that the required task is performed with sufficient accuracy without requiring costly sensors.

IX. CONCLUSIONS

In this paper, we extended our previous work [13] by overcoming its main limitation, i.e., the assumption of diagonal inertia. By building ot top of established methods in control theory and optimization, we proposed a novel and general framework for planning the stiffness and damping matrices for impedance controllers. In contrast with traditional methods,

(a) Low decoupled impedance reduces precision and increases compliance.

(b) High decoupled impedance increases precision and reduces compliance.

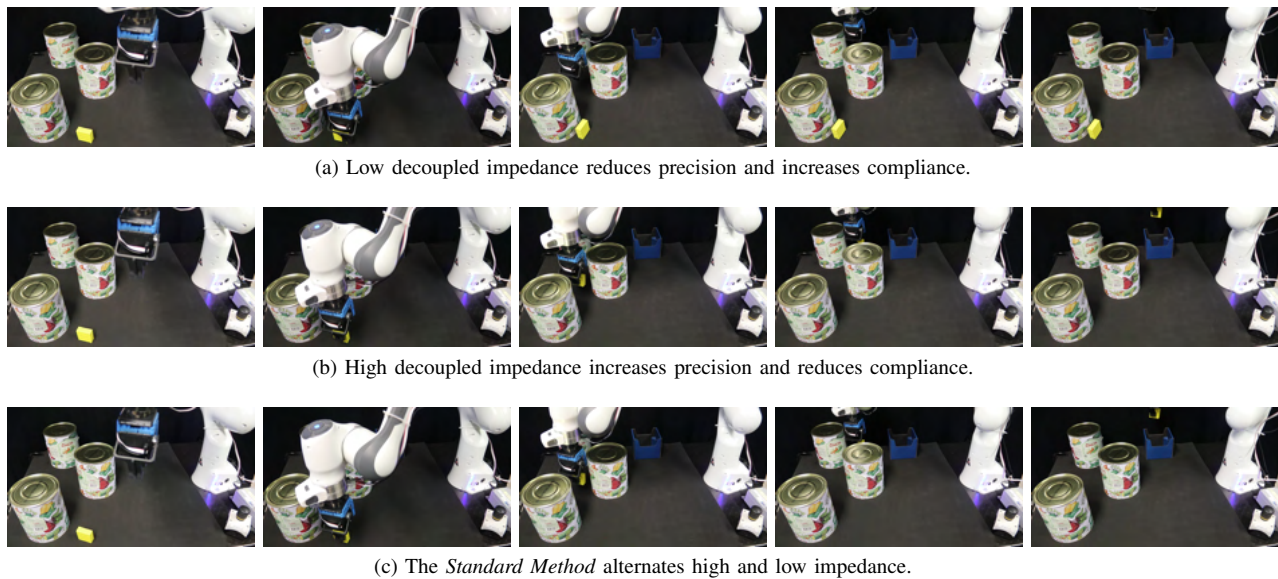(c) The *Standard Method* alternates high and low impedance.

Figure 8. Experiments using the inertia shaping controller in [10]. Fixed-low impedance reduces precision, causing task failure. Fixed-high gains, instead, produce high external forces. The *Standard Method* attempts to balance precision with compliance.

(a) Low coupled impedance reduces precision and increases compliance.

(b) High coupled impedance increases precision and reduces compliance.

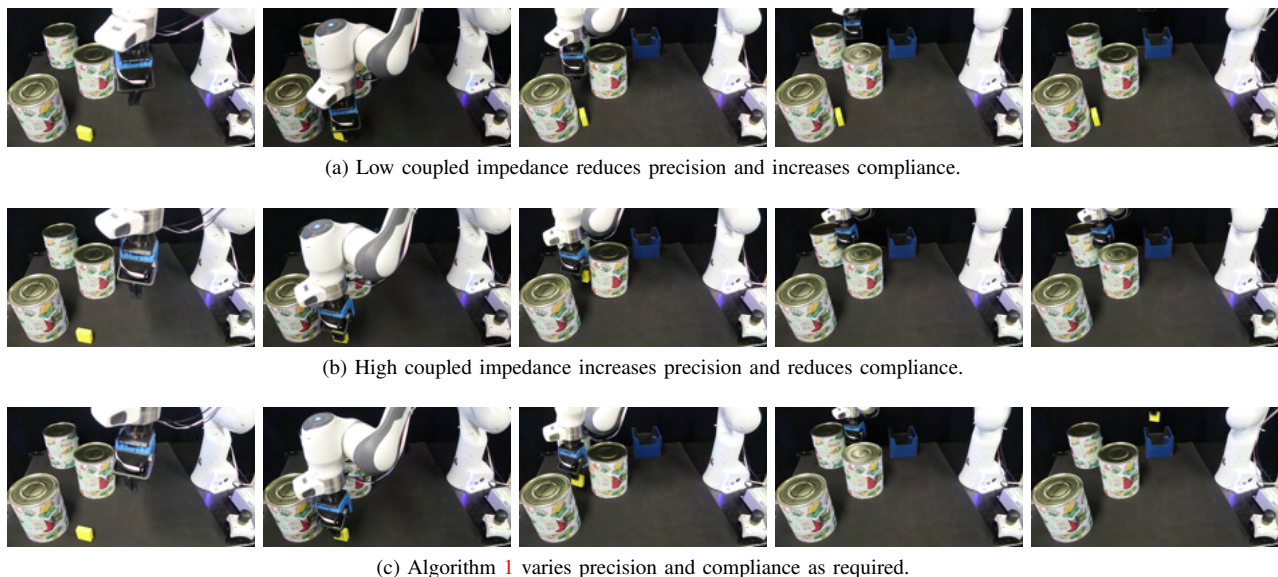(c) Algorithm 1 varies precision and compliance as required.

Figure 9. Experiments using the non inertia shaping controller (similar to [69]). Due to coupling, low gains cause high imprecision and high gains produce external forces that violate the robot safety limits. In both cases, the task fails. Algorithm 1 sets the impedance required to properly balance tracking error reduction and impedance minimization.

we do not rely on the use of expensive sensors to shape the inertia.

After introducing the background and performing a review of the state-of-the-art, we presented our optimization-based solution to the impedance planning problem. Therein, we proposed to minimize some cost related to the impedance of the closed-loop system subject to constraints on the tracking error and on the controller gains. Subsequently, we discussed two possible approaches to solve the minimization by distinguishing the cases of diagonally-dominant and non-diagonally-dominant inertia. In the former case, we provided an analytic formula, which computes the optimal impedance. Instead, the latter case was addressed with numerical methods that produce the stiffness and damping matrices that minimize

the cost and comply with the constraints. Merging these two approaches, we outlined the basic algorithm of our impedance planner. We validated it through extensive experiments on two different robotic platforms and compared it with typical fixed impedance gain cases and a standard impedance choosing method with inertia shaping.

The validity and robustness of our method also with respect to the standard one was clearly shown. Notwithstanding the avoidance of inertia shaping and without using force/torque sensors, our method displayed comparable performance to the standard approach.

Future works will focus on lifting the assumptions of negligible Coriolis-like term and slowly-varying inertia. We will also explore the possibility of techniques that modulate

(a) Frobenius norm of stiffness matrices.

(b) Frobenius norm of damping matrices.

(c) Norm of external force.

(d) Tracking error along $\tilde{x}_1$.

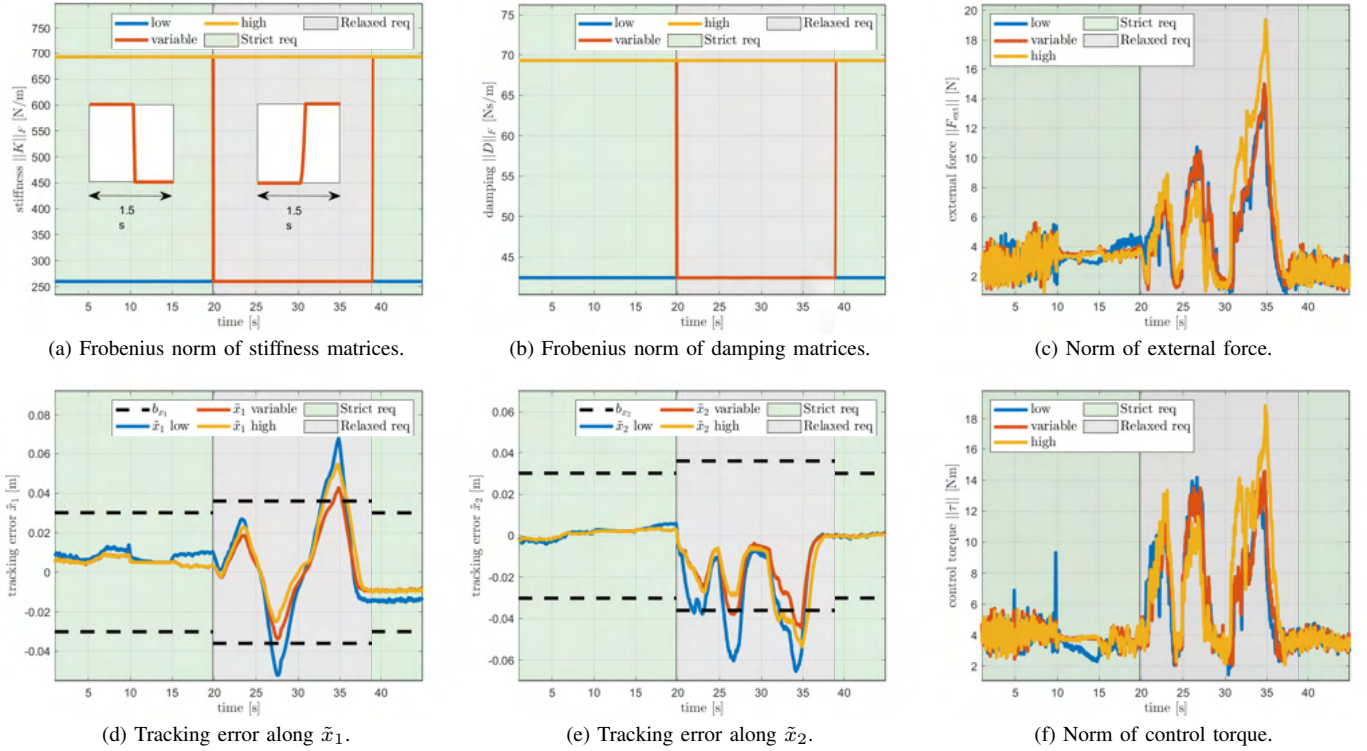(e) Tracking error along $\tilde{x}_2$.

(f) Norm of control torque.

Figure 10. Experiments with the Franka Emika Panda using the inertia shaping controller [10]. The impedance gains for the cases of low, high and variable (*Standard Method*) impedance are shown in (a) and (b). The inserts in (a) show how the *Standard Method* smooths sudden variations using [12] for guaranteeing stability. The norm of the contact forces are plotted in (c). Notice that in real-world scenarios the contact forces are not ideally impulsive. The tracking errors along $\tilde{x}_1$ and $\tilde{x}_2$ together with the boundaries used by the impedance planner are shown in (d) and (e). The norm of the control torque is plotted in (f).

(a) Frobenius norm of stiffness matrices.

(b) Frobenius norm of damping matrices.

(c) Norm of external force.

(d) Tracking error along $\tilde{x}_1$.

(e) Tracking error along $\tilde{x}_2$.
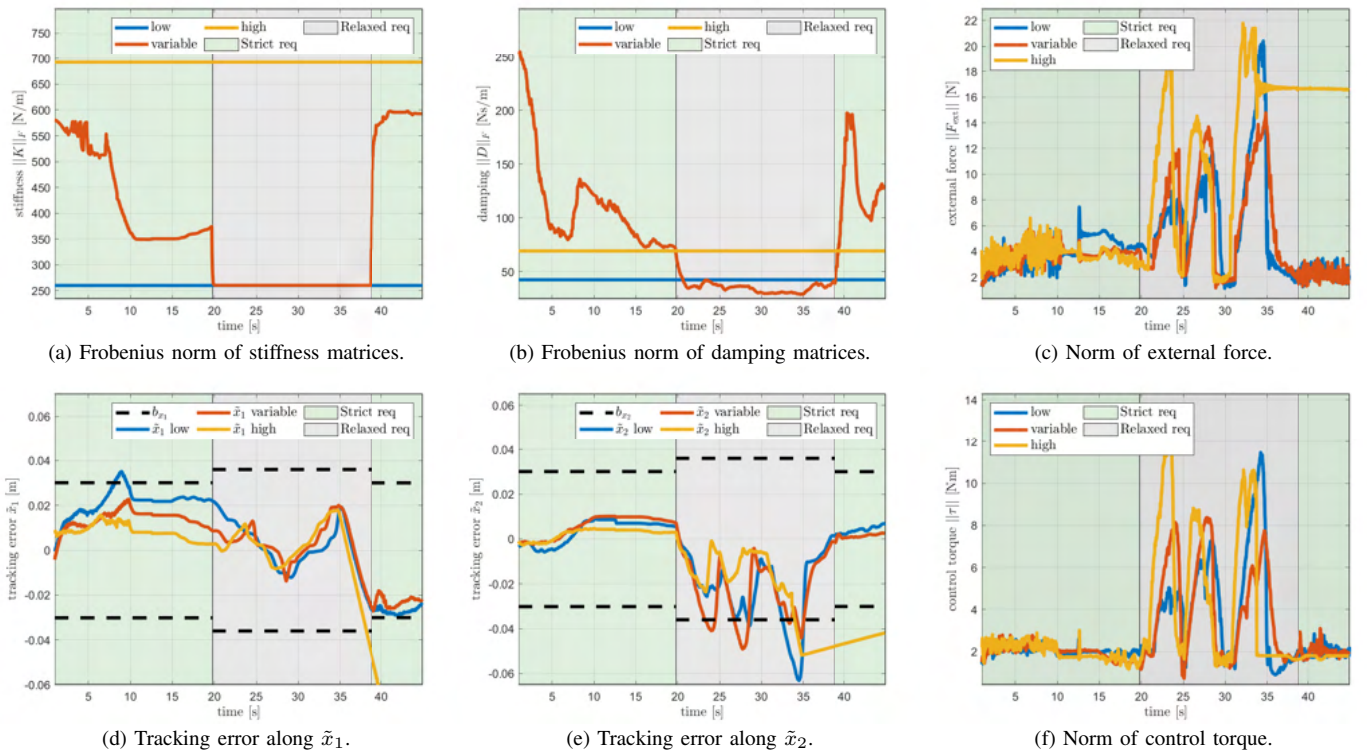
(f) Norm of control torque.

Figure 11. Experiments with the Franka Emika Panda using the non inertia shaping controller [69]. The impedance gains for the cases of low, high and variable (Algorithm 1) impedance are shown in (a) and (b). Here, the damping for the fixed impedance cases are computed with the critically damped condition, as traditionally done. The norm of the contact forces are plotted in (c). For a fair comparison, the fixed gains are the same as in the inertia shaping case. The tracking errors along $\tilde{x}_1$ and $\tilde{x}_2$ together with the boundaries used by the impedance planner are shown in (d) and (e). The norm of the control torque is plotted in (f).

the kinetic energy of the robot to react to peak impact forces. Additionally, based on some insights provided by the experiments on the robots, we will also work on eventually making use of the available sensors in the planning algorithm.

APPENDIX

A. From Impulse Response to Free Response

The combination of free and forced response of (12) is

$$\xi(t) = \phi(t, \mathrm{t}_0)\xi(\mathrm{t}_0) + \int_{\mathrm{t}_0}^{t} \phi(t, \tau)B(\tau)\,\nu(\tau)\mathrm{d}\tau. \quad (49)$$

Here, $\phi(t, \tau)$ is the so-called state-transition matrix [53] and $\nu(t)$ is impulsive with all impulses occurring at t_0: $\nu(t) = \bar{\nu}\,1_6\,\delta_\mathrm{d}(t - \mathrm{t}_0)$, where $1_6 \equiv [1, 1, 1, 1, 1, 1]^\intercal$ and $\delta_\mathrm{d}(t)$ the Dirac delta function. We can apply the *sifting* property of Dirac delta and (49) becomes

$$\xi(t) = \phi(t, \mathrm{t}_0)\xi(\mathrm{t}_0) + \phi(t, \mathrm{t}_0)B(\mathrm{t}_0)\bar{\nu}\,1_6 \quad (50)$$

$$= \phi(t, \mathrm{t}_0)\underbrace{(\xi(\mathrm{t}_0) + B(\mathrm{t}_0)\bar{\nu}\,1_6)}_{\xi'(\mathrm{t}_0)}. \quad (51)$$

Hence, the impulse response from $\xi(t_0)$ is equivalent to the free response from $\xi'(t_0)$. Notice that, given the form of B in (12), $\xi' = \begin{bmatrix} \tilde{x}'^\intercal & \dot{\tilde{x}}'^\intercal \end{bmatrix}^\intercal$ differs from ξ only for the $\dot{\tilde{x}}'^\intercal$. Hence, we justify Remark 2.

B. Free Response of Second Order Linear System

Refactoring the second order single degree of freedom differential equation (37) to draw attention to the damping ratio, we re-write it as

$$\ddot{\mu}_i + \underbrace{2\xi_i\omega_i}_{a_1}\dot{\mu}_i + \underbrace{\omega_i^2}_{a_0}\mu_i = 0. \quad (52)$$

This system is said to be overdamped if $\xi_i > 1$. In this case the modes of the system are real and distinct.

The general form of the free response of (52), for initial conditions $\mu_i(0) = \mu_{0_i}$ and $\dot{\mu}_i(0) = \dot{\mu}_{0_i}$, is provided by

$$\mu_i(t) = \theta_1 e^{\lambda_1 t} + \theta_2 e^{\lambda_2 t}, \quad (53)$$

where, the coefficients are given by

$$\lambda_{1,2} = -\frac{a_1}{2} \pm \frac{\sqrt{a_1^2 - 4a_0}}{2},$$

$$\theta_1 = -\frac{\lambda_2\mu_{0_i} - \dot{\mu}_{0_i}}{\lambda_1 - \lambda_2}, \quad (54)$$

$$\theta_2 = \frac{\lambda_1\mu_{0_i} - \dot{\mu}_{0_i}}{\lambda_1 - \lambda_2}.$$

It is clear that (53) is valid independently of its boundedness, which holds only if the damping coefficient $\xi_i > 0$ and the undamped natural frequency $\omega_i > 0$. To compute the time of peak response, it suffices to differentiate (53) and equate to zero. We get

$$t_{\max} = -\frac{\log\left(-\frac{\theta_1\lambda_1}{\theta_2\lambda_2}\right)}{\lambda_1 - \lambda_2}. \quad (55)$$

Hence, assuming $t_{\max} \geq 0$, the peak value of (53) is

$$\mu_{i_{\max}} = \theta_1\left(-\frac{\theta_1\lambda_1}{\theta_2\lambda_2}\right)^{-\frac{\lambda_1}{\lambda_1 - \lambda_2}} + \theta_2\left(-\frac{\theta_1\lambda_1}{\theta_2\lambda_2}\right)^{-\frac{\lambda_2}{\lambda_1 - \lambda_2}}, \quad (56)$$

A conservative upper-bound can be found for (56) so that the new expression $f_{c_i}(\mu_{0_i}, \dot{\mu}_{0_i}, \cdot)$ is linear w.r.t. the initial states μ_{0_i} and $\dot{\mu}_{0_i}$:

$$\mu_{i_{\max}} \leq \mu_{0_i} + \dot{\mu}_{0_i}\underbrace{\left(\frac{\left(\frac{\lambda_2}{\lambda_1}\right)^{\frac{\lambda_1}{\lambda_1 - \lambda_2}} - \left(\frac{\lambda_2}{\lambda_1}\right)^{\frac{\lambda_2}{\lambda_1 - \lambda_2}}}{\lambda_1 - \lambda_2}\right)}_{f_{c_i}(\mu_{0_i}, \dot{\mu}_{0_i}, \cdot)}. \quad (57)$$

C. Example of Bound Choosing Method

The set $\mathcal{S} = \{l_{k_{i,j}}, u_{k_{i,j}}, l_{d_{i,j}}, u_{d_{i,j}}, l_{\tilde{x}_{0_i}}, u_{\tilde{x}_{0_i}}, l_{\dot{\tilde{x}}_{0_i}}, u_{\dot{\tilde{x}}_{0_i}}, b_i\}$. Its first four parameters depend on the maximum and minimum controller gains ($K_{\max}$, $K_{\min}$, $D_{\max}$, and $D_{\min}$). The remaining are related to the tracking error $\tilde{x}$ and its derivative $\dot{\tilde{x}}$.

The below procedure can be followed to choose them:
1) From the task-specific required precision, choose b_i. For instance, if the task regards grasping, b_i is the needed tolerance. Instead, if the controller regulates the CoM of a walking robot, b_i might be related to the physical feasibility of the CoM trajectory.
2) Choose $l_{\tilde{x}_{0_i}}$, $u_{\tilde{x}_{0_i}}$, $l_{\dot{\tilde{x}}_{0_i}}$, and $u_{\dot{\tilde{x}}_{0_i}}$ based on the maximum position and velocity errors, $\tilde{x}_{\max}$ and $\dot{\tilde{x}}_{\max}$, that occur while using the considered impedance controller with the commonly used fixed gains. For instance, $l_{\tilde{x}_{0_i}} = -|\tilde{x}_{\max}|$, $u_{\tilde{x}_{0_i}} = |\tilde{x}_{\max}|$, $l_{\dot{\tilde{x}}_{0_i}} = -|\dot{\tilde{x}}_{\max}|$, and $u_{\dot{\tilde{x}}_{0_i}} = |\dot{\tilde{x}}_{\max}|$. Alternatively, $l_{\dot{\tilde{x}}_{0_i}}$ and $u_{\dot{\tilde{x}}_{0_i}}$ can also be chosen from an estimate of the maximum expected (impulsive) contact force by leveraging Remark 2 (see also Appendix A).
3) Clearly, it should hold that the bounds b_i on the tracking error are above the bound on the initial error $u_{\tilde{x}_{0_i}}$: i.e., $u_{\tilde{x}_{0_i}} \leq b_i$. Otherwise, the tracking error is not within the bounds at the initial instant.
4) Choose $D_{\max}$ and $D_{\min}$ to enforce a critically damped behaviour: $D_{\max} = 2\Lambda_{\max}^{\frac{1}{2}}K_{\max}\Lambda_{\max}^{\frac{1}{2}}$ and $D_{\min} = 2\Lambda_{\min}^{\frac{1}{2}}K_{\min}\Lambda_{\min}^{\frac{1}{2}}$. Here, $\Lambda_{\max}$ and $\Lambda_{\min}$ are respectively the maximum and minimum Cartesian inertia w.r.t. some cost: for instance, $\|\Lambda(q)\|_F$.

    More in detail, we define the operator $(\cdot)_{\max}$ that, applied to a matrix $A(q)$ function of q, finds

    $$q^\star = \arg\max_q \|A(q)\|_F.$$

    Then, $A_{\max} = A(q^\star)$. The operator $(\cdot)_{\min}$ is defined analogously with the only difference that the norm is minimized. Similarly, also other matrices of the model can be maximized/minimized. Notice that the matrices obtained by applying the operators $(\cdot)_{\min}$ and $(\cdot)_{\max}$ lead to under or overestimations of the matrix itself.
5) Finally, choose $K_{\max}$ and $K_{\min}$ following the common rationale of choosing $K_{\max}$ so that control limits are not violated and $K_{\min}$ high enough to compensate for model uncertainties.

    On the impedance control law (3)-(5), we assume quasi-static conditions: this yields

    $$\tau = J^\intercal(q)F_\tau + G(q), \quad (58)$$

and

$$F_\tau = -K\tilde{x}. \tag{59}$$

The following can approximate analysis be performed:

1) Choosing $K_{\max}$: Scale the maximum allowed torque $\tau_{\max}$ of a safety factor $0 < \delta_s < 1$. Inverting (58) and considering a worst-case scenario, get the maximum admissible Cartesian force:

$$F_{\tau_{\max}} = (J_{\max}^\mathsf{T})^\dagger(\delta_s \tau_{\max} + G_{\max}). \tag{60}$$

Here, $J_{\max}$ and $G_{\max}$ are respectively obtained by applying the operator $(\cdot)_{\max}$ to the Jacobian and gravity torques. Notice that $F_{\tau_{\max}}$ is an conservative estimate of the maximum allowed F_τ that would not violate $\tau_{\max}$. From (59), equation (60) should match

$$F_{\tau_{\max}} = -K_{\max}\tilde{x}_{\max}. \tag{61}$$

Equating (60) and (61) leads to

$$(J_{\max}^\mathsf{T})^\dagger(\delta_s \tau_{\max} + G_{\max}) = -K_{\max}\tilde{x}_{\max}, \tag{62}$$

Equality (62) can be solved numerically (recall that this is done only once offline) with the only unknown $K_{\max}$ constrained to be positive definite (e.g., using Cholesky decomposition).

2) Choosing $K_{\min}$: Assuming model uncertainties only on the dynamic parameters (since kinematic quantities are easier to identify), model them as multiplicative uncertainties: e.g., $\hat{G}(q) = (I + \Delta)G(q)$ is the estimated gravity torques with a relative error Δ.

Within the quasi-static assumption, the control law $\hat{\tau}$ using the estimated model acts on the robot as follows:

$$\cancel{B\ddot{q}}^0 + \cancel{C\dot{q}}^0 + G = \underbrace{J^\mathsf{T}F_\tau + \cancel{\hat{C}\dot{q}}^0 + \hat{G}}_{\hat{\tau}}. \tag{63}$$

Solving for F_τ gives $F_{\tau_{\min}}$, an under estimate of the minimum necessary F_τ that would provide robustness to model uncertainties.

$$F_{\tau_{\min}} = (J_{\max}^\mathsf{T})^\dagger(-\Delta G_{\max}), \tag{64}$$

which, together with (59), yields the equality

$$(J_{\max}^\mathsf{T})^\dagger(-\Delta G_{\max}) = -K_{\min}\tilde{x}_{\mathrm{avg}}. \tag{65}$$

Here, the unknown is $K_{\min}$ and $\tilde{x}_{\mathrm{avg}}$ is an average tracking error. Also (65) can be solved numerically.

In practice, if estimates of maximum and minimum interaction forces are already provided, these can be directly used instead of $F_{\tau_{\max}}$ and $F_{\tau_{\min}}$ to compute $K_{\max}$ and $K_{\min}$, respectively.

It is worth mentioning that the presented procedure is approximate because the $F_{\tau_{\min}}$ and $F_{\tau_{\max}}$ are not the actual minimum/maximum wrench capabilities of the robot. This is because of the under/overestimations performed during the procedure. Indeed, to properly translate joint capabilities, such as joint torque limits, to the Cartesian space (for instance, to maximum/minimum wrenches), complicated techniques such as vertices enumeration are required [74].

However, the procedure eases tuning by reducing the parameters to be tuned to just the tracking error bound b_i. All the other parameters are computed automatically from measurements or from the knowledge of the robot hardware or its model.

Finally, we stress that the above procedure is in no way a required component of the proposed framework. It is just one of many possible ways to choose the set $\mathcal{S}$.

REFERENCES

[1] A. Hentout, M. Aouache, A. Maoudj, and I. Akli, "Human–robot interaction in industrial collaborative robotics: a literature review of the decade 2008–2017," *Advanced Robotics*, vol. 33, no. 15-16, pp. 764–799, 2019.

[2] S. Shepherd and A. Buchstab, "Kuka robots on-site," in *Robotic Fabrication in Architecture, Art and Design 2014*. Springer, 2014, pp. 373–380.

[3] M. Hutter, C. Gehring, D. Jud, A. Lauber, C. D. Bellicoso, V. Tsounis, J. Hwangbo, K. Bodie, P. Fankhauser, M. Bloesch *et al.*, "Anymal-a highly mobile and dynamic quadrupedal robot," in *2016 IEEE/RSJ International Conference on Intelligent Robots and Systems (IROS)*. IEEE, 2016, pp. 38–44.

[4] C. Della Santina, M. G. Catalano, and A. Bicchi, *Soft Robots*. Springer Berlin Heidelberg, 2020, pp. 1–14.

[5] M. W. Spong, "Modeling and Control of Elastic Joint Robots," *Journal of Dynamic Systems, Measurement, and Control*, vol. 109, no. 4, pp. 310–318, 12 1987.

[6] M. Moallem, R. V. Patel, and K. Khorasani, *Flexible-link robot manipulators*. Springer, 2000.

[7] S. Wolf, G. Grioli, O. Eiberger, W. Friedl, M. Grebenstein, H. Höppner, E. Burdet, D. G. Caldwell, R. Carloni, M. G. Catalano *et al.*, "Variable stiffness actuators: Review on design and components," *IEEE/ASME transactions on mechatronics*, vol. 21, no. 5, pp. 2418–2430, 2015.

[8] B. Vanderborght, A. Albu-Schäffer, A. Bicchi, E. Burdet, D. G. Caldwell, R. Carloni, M. Catalano, O. Eiberger, W. Friedl, G. Ganesh *et al.*, "Variable impedance actuators: A review," *Robotics and autonomous systems*, vol. 61, no. 12, pp. 1601–1614, 2013.

[9] N. Hogan, "Impedance control: An approach to manipulation: Part i—theory," *Journal of Dynamic Systems, Measurement, and Control*, vol. 107, no. 1, pp. 1–7, 03 1985.

[10] A. Albu-Schaffer, C. Ott, U. Frese, and G. Hirzinger, "Cartesian impedance control of redundant robots: Recent results with the dlr-light-weight-arms," in *2003 IEEE International Conference on Robotics and Automation*, vol. 3. IEEE, 2003, pp. 3704–3709.

[11] F. Ficuciello, A. Romano, L. Villani, and B. Siciliano, "Cartesian impedance control of redundant manipulators for human-robot co-manipulation," in *2014 IEEE/RSJ International Conference on Intelligent Robots and Systems*. IEEE, 2014, pp. 2120–2125.

[12] K. Kronander and A. Billard, "Stability considerations for variable impedance control," *IEEE Transactions on Robotics*, vol. 32, no. 5, pp. 1298–1305, 2016.

[13] F. Angelini, G. Xin, W. J. Wolfslag, C. Tiseo, M. Mistry, M. Garabini, A. Bicchi, and S. Vijayakumar, "Online optimal impedance planning for legged robots," in *IEEE International Conference on Intelligent Robots and Systems*, 2019.

[14] B. Siciliano, L. Sciavicco, L. Villani, and G. Oriolo, *Robotics: modelling, planning and control*. Springer Science & Business Media, 2010.

[15] A. Albu-Schaffer and G. Hirzinger, "Cartesian impedance control techniques for torque controlled light-weight robots," in *Proceedings 2002 IEEE International Conference on Robotics and Automation (Cat. No. 02CH37292)*, vol. 1. IEEE, 2002, pp. 657–663.

[16] H.-C. Lin, J. Smith, K. K. Babarahmati, N. Dehio, and M. Mistry, "A projected inverse dynamics approach for multi-arm cartesian impedance control," in *2018 IEEE International Conference on Robotics and Automation (ICRA)*. IEEE, 2018, pp. 1–5.

[17] A. Dietrich, K. Bussmann, F. Petit, P. Kotyczka, C. Ott, B. Lohmann, and A. Albu-Schäffer, "Whole-body impedance control of wheeled mobile manipulators," *Autonomous Robots*, vol. 40, no. 3, pp. 505–517, 2016.

[18] H.-O. Lim, S. A. Setiawan, and A. Takanishi, "Position-based impedance control of a biped humanoid robot," *Advanced Robotics*, vol. 18, no. 4, pp. 415–435, 2004.

[19] G. Xin, H.-C. Lin, J. Smith, O. Cebe, and M. Mistry, "A model-based hierarchical controller for legged systems subject to external disturbances," in *2018 IEEE International Conference on Robotics and Automation (ICRA)*. IEEE, 2018, pp. 4375–4382.

[20] N. Hogan, "Impedance control of industrial robots," *Robotics and Computer-Integrated Manufacturing*, vol. 1, no. 1, pp. 97–113, 1984.

[21] D. Surdilovic, "Contact transition stability in the impedance control," in *Proceedings of International Conference on Robotics and Automation*, vol. 1. IEEE, 1997, pp. 847–852.

[22] D. Surdilovic and Z. Cojbasic, "Robust robot compliant motion control using intelligent adaptive impedance approach," in *Proceedings 1999 IEEE International Conference on Robotics and Automation (Cat. No. 99CH36288C)*, vol. 3. IEEE, 1999, pp. 2128–2133.

[23] B.-H. Yang and H. Asada, "Progressive learning and its application to robot impedance learning," *IEEE transactions on neural networks*, vol. 7, no. 4, pp. 941–952, 1996.

[24] M. Uemura and S. Kawamura, "Resonance-based motion control method for multi-joint robot through combining stiffness adaptation and iterative learning control," in *2009 IEEE International Conference on Robotics and Automation*. IEEE, 2009, pp. 1543–1548.

[25] T. Yamawaki, H. Ishikawa, and M. Yashima, "Iterative learning of variable impedance control for human-robot cooperation," in *2016 IEEE/RSJ International Conference on Intelligent Robots and Systems (IROS)*. IEEE, 2016, pp. 839–844.

[26] Y. Li, G. Ganesh, N. Jarrassé, S. Haddadin, A. Albu-Schaeffer, and E. Burdet, "Force, impedance, and trajectory learning for contact tooling and haptic identification," *IEEE Transactions on Robotics*, vol. 34, no. 5, pp. 1170–1182, 2018.

[27] M. Bednarczyk, H. Omran, and B. Bayle, "Model predictive impedance control," in *2020 IEEE International Conference on Robotics and Automation (ICRA)*. IEEE, 2020, pp. 4702–4708.

[28] M. Bednarczyk, H. Omran, and B. Bayle, "Passivity filter for variable impedance control," in *2020 IEEE/RSJ International Conference on Intelligent Robots and Systems (IROS)*. IEEE, 2020, pp. 7159–7164.

[29] E. Gribovskaya, A. Kheddar, and A. Billard, "Motion learning and adaptive impedance for robot control during physical interaction with humans," in *2011 IEEE International Conference on Robotics and Automation*. IEEE, 2011, pp. 4326–4332.

[30] M. Li, H. Yin, K. Tahara, and A. Billard, "Learning object-level impedance control for robust grasping and dexterous manipulation," in *2014 IEEE International Conference on Robotics and Automation (ICRA)*. IEEE, 2014, pp. 6784–6791.

[31] C. Yang, G. Ganesh, S. Haddadin, S. Parusel, A. Albu-Schaeffer, and E. Burdet, "Human-like adaptation of force and impedance in stable and unstable interactions," *IEEE transactions on robotics*, vol. 27, no. 5, pp. 918–930, 2011.

[32] Y. Wu, F. Zhao, T. Tao, and A. Ajoudani, "A framework for autonomous impedance regulation of robots based on imitation learning and optimal control," *IEEE Robotics and Automation Letters*, 2020.

[33] T. Tsuji, K. Ito, and P. G. Morasso, "Neural network learning of robot arm impedance in operational space," *IEEE Transactions on Systems, Man, and Cybernetics, Part B (Cybernetics)*, vol. 26, no. 2, pp. 290–298, 1996.

[34] J. Buchli, F. Stulp, E. Theodorou, and S. Schaal, "Learning variable impedance control," *The International Journal of Robotics Research*, vol. 30, no. 7, pp. 820–833, 2011.

[35] J. Xu and Z. Zhu, "Reinforced continual learning," in *Proceedings of the 32nd International Conference on Neural Information Processing Systems*, ser. NIPS'18. Red Hook, NY, USA: Curran Associates Inc., 2018, p. 907–916.

[36] H. Mehdi and O. Boubaker, "Impedance controller tuned by particle swarm optimization for robotic arms," *International Journal of Advanced Robotic Systems*, vol. 8, no. 5, p. 57, 2011.

[37] G. Gasparri, F. Fabiani, M. Garabini, L. Pallottino, M. Catalano, G. Grioli, R. Persichin, and A. Bicchi, "Robust optimization of system compliance for physical interaction in uncertain scenarios," in *2016 IEEE-RAS 16th International Conference on Humanoid Robots (Humanoids)*. IEEE, 2016, pp. 911–918.

[38] J. Nakanishi, A. Radulescu, and S. Vijayakumar, "Spatio-temporal optimization of multi-phase movements: Dealing with contacts and switching dynamics," in *2013 IEEE/RSJ International Conference on Intelligent Robots and Systems*. IEEE, 2013, pp. 5100–5107.

[39] D. J. Braun, F. Petit, F. Huber, S. Haddadin, P. Van Der Smagt, A. Albu-Schäffer, and S. Vijayakumar, "Robots driven by compliant actuators: Optimal control under actuation constraints," *IEEE Transactions on Robotics*, vol. 29, no. 5, pp. 1085–1101, 2013.

[40] M. Howard, D. J. Braun, and S. Vijayakumar, "Transferring human impedance behavior to heterogeneous variable impedance actuators," *IEEE Transactions on Robotics*, vol. 29, no. 4, pp. 847–862, 2013.

[41] D. Braun, M. Howard, and S. Vijayakumar, "Optimal variable stiffness control: formulation and application to explosive movement tasks," *Autonomous Robots*, vol. 33, no. 3, pp. 237–253, 2012.

[42] A. Taherifar, G. Vossoughi, and A. Selk Ghafari, "Optimal target impedance selection of the robot interacting with human," *Advanced Robotics*, vol. 31, no. 8, pp. 428–440, 2017.

[43] T. Tsumugiwa, R. Yokogawa, and K. Hara, "Variable impedance control with regard to working process for man-machine cooperation-work system," in *Proceedings 2001 IEEE/RSJ International Conference on Intelligent Robots and Systems. Expanding the Societal Role of Robotics in the the Next Millennium (Cat. No. 01CH37180)*, vol. 3. IEEE, 2001, pp. 1564–1569.

[44] T. Tsumugiwa, R. Yokogawa, and K. Hara, "Variable impedance control based on estimation of human arm stiffness for human-robot cooperative calligraphic task," in *Proceedings 2002 IEEE International Conference on Robotics and Automation (Cat. No. 02CH37292)*, vol. 1. IEEE, 2002, pp. 644–650.

[45] F. Ficuciello, L. Villani, and B. Siciliano, "Variable impedance control of redundant manipulators for intuitive human–robot physical interaction," *IEEE Transactions on Robotics*, vol. 31, no. 4, pp. 850–863, 2015.

[46] E. Spyrakos-Papastavridis, N. Kashiri, J. Lee, N. G. Tsagarakis, and D. G. Caldwell, "Online impedance parameter tuning for compliant biped balancing," in *2015 IEEE-RAS 15th International Conference on Humanoid Robots (Humanoids)*. IEEE, 2015, pp. 210–216.

[47] E. Spyrakos-Papastavridis, P. R. Childs, and N. G. Tsagarakis, "Variable impedance walking using time-varying lyapunov stability margins," in *2017 IEEE-RAS 17th International Conference on Humanoid Robotics (Humanoids)*. IEEE, 2017, pp. 318–323.

[48] E. Spyrakos-Papastavridis, N. Kashiri, P. R. Childs, and N. G. Tsagarakis, "Online impedance regulation techniques for compliant humanoid balancing," *Robotics and Autonomous Systems*, vol. 104, pp. 85–98, 2018.

[49] P. Balatti, D. Kanoulas, G. F. Rigano, L. Muratore, N. G. Tsagarakis, and A. Ajoudani, "A self-tuning impedance controller for autonomous robotic manipulation," in *2018 IEEE/RSJ International Conference on Intelligent Robots and Systems (IROS)*. IEEE, 2018, pp. 5885–5891.

[50] P. Balatti, D. Kanoulas, N. Tsagarakis, and A. Ajoudani, "A method for autonomous robotic manipulation through exploratory interactions with uncertain environments," *Autonomous Robots*, vol. 44, no. 8, pp. 1395–1410, 2020.

[51] D. Bertsimas, D. B. Brown, and C. Caramanis, "Theory and applications of robust optimization," *SIAM review*, vol. 53, no. 3, pp. 464–501, 2011.

[52] J. P. Hespanha, *Linear systems theory*. Princeton university press, 2018.

[53] H. M. Moya-Cessa and F. Soto-Eguibar, *Differential equations: an operational approach*. Rinton Press, Incorporated, 2011.

[54] S. Boyd, S. P. Boyd, and L. Vandenberghe, *Convex optimization*. Cambridge university press, 2004.

[55] A. O. Ignatyev, "Stability of a linear oscillator with variable parameters," 1997.

[56] V. Gabrel, C. Murat, and A. Thiele, "Recent advances in robust optimization: An overview," *European journal of operational research*, vol. 235, no. 3, pp. 471–483, 2014.

[57] S. Leyffer, M. Menickelly, T. Munson, C. Vanaret, and S. M. Wild, "A survey of nonlinear robust optimization," *INFOR: Information Systems and Operational Research*, pp. 1–32, 2020.

[58] T. Caughey and M. E. J. O'Kelly, "Classical normal modes in damped linear dynamic systems," *Journal of Applied Mechanics*, 1965.

[59] D. J. Inman, *Vibration with control*. John Wiley & Sons, 2017.

[60] A. G. Nahapetyan, "Bilinear programming," 2009.

[61] M. F. Anjos and J. B. Lasserre, *Handbook on semidefinite, conic and polynomial optimization*. Springer Science & Business Media, 2011, vol. 166.

[62] A. Ruszczynski, *Nonlinear optimization*. Princeton university press, 2011.

[63] J. Rosen, "The gradient projection method for nonlinear programming. part ii. nonlinear constraints," *Journal of the Society for Industrial and Applied Mathematics*, vol. 9, no. 4, pp. 514–532, 1961.

[64] H. D. Sherali and A. Alameddine, "A new reformulation-linearization technique for bilinear programming problems," *Journal of Global optimization*, vol. 2, no. 4, pp. 379–410, 1992.

[65] H. D. Sherali and C. H. Tuncbilek, "A global optimization algorithm for polynomial programming problems using a reformulation-linearization technique," *Journal of Global Optimization*, vol. 2, no. 1, pp. 101–112, 1992.

[66] I. Pólik and T. Terlaky, "Interior point methods for nonlinear optimization," in *Nonlinear optimization*. Springer, 2010, pp. 215–276.

[67] N. I. Gould and S. Leyffer, "An introduction to algorithms for nonlinear optimization," in *Frontiers in numerical analysis*. Springer, 2003, pp. 109–197.

[68] N. S. Rau, *Optimization principles: practical applications to the operation and markets of the electric power industry*. John Wiley & Sons, 2003, vol. 16.

[69] C. Ott, *Cartesian impedance control of redundant and flexible-joint robots*. Springer, 2008.

[70] Franka Emika, "The Robot System - Franka Emika," https://www.franka.de/robot-system, 2021, [Accessed 12-12-2021].

[71] ATI Industrial Automation, "F/T Sensor Mini45," https://www.ati-ia.com/products/ft/ft_models.aspx?id=Mini45, 2021, [Accessed 12-12-2021].

[72] QB Robotics, "The QB SoftClaw," https://qbrobotics.com/products/qb-softclaw/qb-softclaw/, 2021, [Accessed 12-12-2021].

[73] P. Fankhauser, M. Bjelonic, C. D. Bellicoso, T. Miki, and M. Hutter, "Robust rough-terrain locomotion with a quadrupedal robot," in *2018 IEEE International Conference on Robotics and Automation (ICRA)*. IEEE, 2018, pp. 1–8.

[74] P. Chiacchio, Y. Bouffard-Vercelli, and F. Pierrot, "Evaluation of force capabilities for redundant manipulators," in *Proceedings of IEEE International Conference on Robotics and Automation*, vol. 4. IEEE, 1996, pp. 3520–3525.

Michael Mistry received the Ph.D. degree in computer science from Stefan Schaals CLMC Lab, University of Southern California in 2009. He has been a Senior Lecturer in robotics with the School of Computer Science, University of Birmingham, a Postdoc with the Disney Research Lab, Carnegie Mellon University, and a Researcher with the ATR Computational Neuroscience Lab, Kyoto. He is currently a Professor in Robotics with the School of Informatics, University of Edinburgh, where he is also a member of the Edinburgh Centre for Robotics.

Sethu Vijayakumar is currently the Professor of Robotics with The University of Edinburgh, an Adjunct Faculty with the University of Southern California and the Founding Director with the Edinburgh Centre for Robotics. Prof. Vijayakumar helps shape and drive the national Robotics and Autonomous Systems (RAS) agenda in his recent role as the Programme Co-Director for Artificial Intelligence (AI) with The Alan Turing Institute, the UKs national institute for data science and AI. He is a Fellow of the Royal Society of Edinburgh, a Judge on BBC Robot Wars and winner of the 2015 Tam Dalyell Prize for excellence in engaging the public with science.
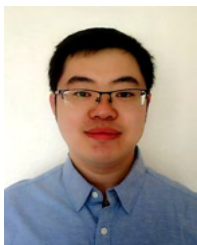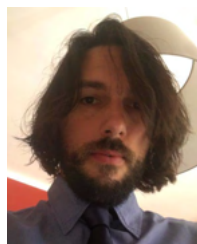
Mathew Jose Pollayil received the B.S. degree in biomedical engineering and the M.S. degree (cum laude) in robotics and automation engineering from the University of Pisa, Pisa, Italy, in 2014 and 2018, respectively, where he also received the Ph.D. degree (cum laude) in robotics with the Research Center "E. Piaggio" and with the Dipartimento di Ingegneria dell'Informazione, in 2022. He is also an Affiliated Researcher with the Italian Institute of Technology, Genoa, Italy. His main research interests include nonlinear control of robots, impedance planning, and motion planning of elastic quadrupeds.

Antonio Bicchi is a scientist interested in robotics and intelligent machines. He holds a chair in Robotics at the University of Pisa, leads the Soft Robotics Laboratory at the Italian Institute of Technology in Genova, and is an Adjunct Professor at Arizona State University. His work has been recognized with many international awards and has earned him four prestigious grants from the European Research Council (ERC). He launched initiatives such as the WorldHaptics conference series, the IEEE Robotics and Automation Letters, and the Italian Institute of Robotics and Intelligent Machines.

Franco Angelini received the B.S. degree in computer engineering in 2013 and the M.S. degree (cum laude) in automation and robotics engineering in 2016, and the Ph.D. degree (cum laude) in robotics in 2020, all from the University of Pisa, Pisa, Italy. He is currently an Assistant Professor with the Department of Information Engineering, University of Pisa. His main research interests include control of soft robotic systems, robotic environmental monitoring, and impedance planning.

Manolo Garabini graduated in Mechanical Engineering and received the Ph.D. in Robotics from the University of Pisa where he is currently an Assistant Professor. His research interests include the design, planning and control of soft adaptive robots. He contributed to the realization of Variable Stiffness Actuators and of the humanoid robot WALK-MAN. Currently was Principal Investigator in the THING H2020 EU Research Project for the University of Pisa, and currently the coordinator of the Dysturbance H2020 Eurobench sub-project and the NI H2020 EU Research Project.

Guiyang Xin received the M.Sc. degree in mechanical engineering from the China University of Geosciences, Wuhan, China, in 2012 and the Ph.D. degree in mechanical engineering from the Central South University, Changsha, China, in 2018. He is currently an Associate Professor at the Dalian University of Technology, Dalian, China. From 2018 to 2021, he was a Postdoctoral Researcher in the Institute of Perception, Action and Behaviour at the University of Edinburgh, Edinburgh, U.K.. His research interests include legged robotics, impedance control, optimization-based control and teleoperation.